

Journal Pre-proof

Discovery of brain permeable 2-Azabicyclo[2.2.2]octane sulfonamides as a novel class of presenilin-1 selective γ -secretase inhibitors

Rajeshwar Narlawar, Lutgarde Serneels, Celia Gaffric, Harrie J.M. Gijssen, Bart De Strooper, François Bischoff



PII: S0223-5234(23)00692-X

DOI: <https://doi.org/10.1016/j.ejmech.2023.115725>

Reference: EJMECH 115725

To appear in: *European Journal of Medicinal Chemistry*

Received Date: 26 April 2023

Revised Date: 4 August 2023

Accepted Date: 13 August 2023

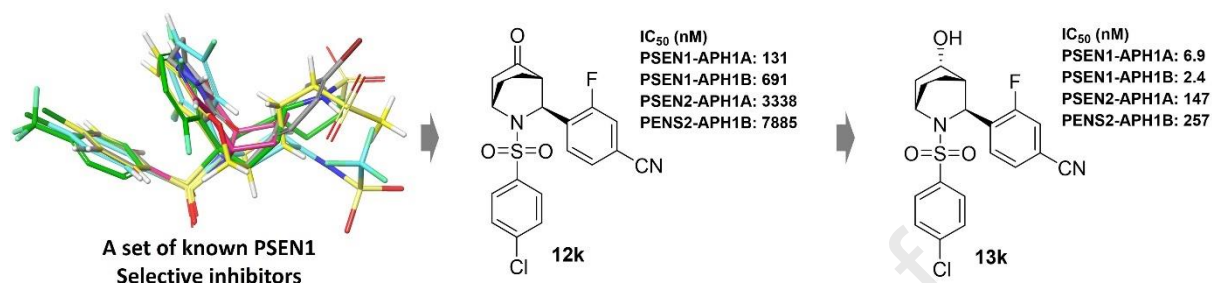
Please cite this article as: R. Narlawar, L. Serneels, C. Gaffric, H.J.M. Gijssen, B. De Strooper, Franç. Bischoff, Discovery of brain permeable 2-Azabicyclo[2.2.2]octane sulfonamides as a novel class of presenilin-1 selective γ -secretase inhibitors, *European Journal of Medicinal Chemistry* (2023), doi: <https://doi.org/10.1016/j.ejmech.2023.115725>.

This is a PDF file of an article that has undergone enhancements after acceptance, such as the addition of a cover page and metadata, and formatting for readability, but it is not yet the definitive version of record. This version will undergo additional copyediting, typesetting and review before it is published in its final form, but we are providing this version to give early visibility of the article. Please note that, during the production process, errors may be discovered which could affect the content, and all legal disclaimers that apply to the journal pertain.

© 2023 Published by Elsevier Masson SAS.

Graphical Abstract

Discovery of brain permeable 2-Azabicyclo[2.2.2]octane sulfonamides as a novel class of presenilin-1 selective γ -secretase inhibitors



Discovery of brain permeable 2-Azabicyclo[2.2.2]octane sulfonamides as a novel class of presenilin-1 selective γ -secretase inhibitors

Authors:

Rajeshwar Narlawar,^{‡,||*} Lutgarde Serneels,[†] Celia Gaffric,[‡] Harrie J. M. Gijsen,[‡] Bart De Strooper^{†,||,§} and François Bischoff.^{‡*}

Affiliations:

[†] VIB Center for Brain and Disease Research, Leuven, Belgium

^{||} KU Leuven, Department of Neurosciences, Leuven Institute for Neuroscience and Disease, (LIND), Leuven, Belgium

[‡] Discovery Chemistry, Discovery Sciences, Janssen Research & Development, Janssen Pharmaceutica NV, Turnhoutseweg 30, B-2340, Beerse, Belgium

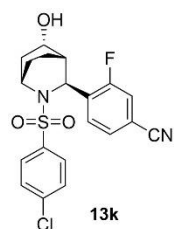
[§] Dementia Research Institute, University College London, London, UK

Address for correspondence

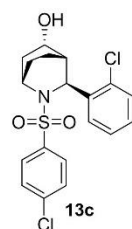
[‡]Discovery Chemistry, Discovery Sciences, Janssen Research & Development, Janssen Pharmaceutica NV, Turnhoutseweg 30, B-2340, Beerse, Belgium

rajnarlawar@gmail.com

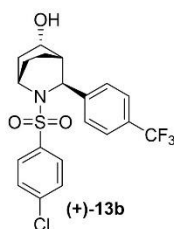
fbischof@its.jnj.com

Abstract:

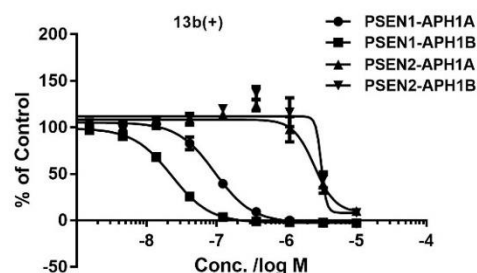
IC₅₀ (nM)
 PSEN1-APH1A: 6.9
 PSEN1-APH1B: 2.4
 PSEN2-APH1A: 147
 PSEN2-APH1B: 257



IC₅₀ (nM)
 PSEN1-APH1A: 12
 PSEN1-APH1B: 3
 PSEN2-APH1A: 131
 PSEN2-APH1B: 214



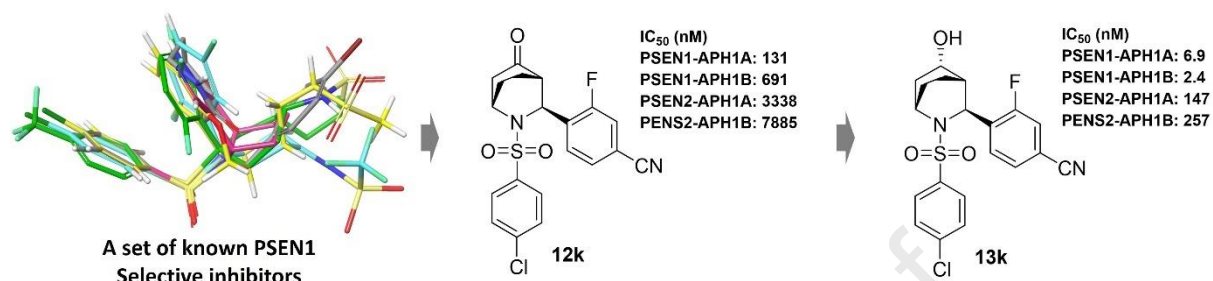
IC₅₀ (nM)
 PSEN1-APH1A: 19
 PSEN1-APH1B: 5.5
 PSEN2-APH1A: 1950
 PSEN2-APH1B: 2138



This paper describes the rational design, synthesis, structure-activity relationship (SAR), and biological profile of presenilin-1 (PSEN-1) complex selective γ -secretase inhibitors, assessed for selectivity using a unique set of four γ -secretase subtype complexes. A set of known PSEN-1 selective γ -Secretase inhibitors (GSIs) was analyzed to understand the pharmacophoric features required for selective inhibition. Conformational modeling suggests that a characteristic 'U' shape orientation between aromatic sulfone/sulfonamide and aryl ring is crucial for PSEN-1 selectivity and potency. Using these insights, a series of brain-penetrant 2-azabicyclo[2,2,2]octane sulfonamides was devised and synthesized as a new class of PSEN-1 selective inhibitors. Compounds **13c** and **13k** displayed high potency towards PSEN1-APH1B complex but moderate selectivity towards PSEN2 complexes. However, compound (+)-**13b** displayed low nanomolar potency towards the PSEN1-APH1B complex, little (~4-fold) selectivity towards PSEN1-APH1A, and high selectivity (>350-fold) versus PSEN2 complexes. Excellent brain penetration, no significant CYP inhibition, or cardiotoxicity, good solubility, and permeability make (+)-**13b** an excellent candidate for further lead optimization.

Graphical Abstract

Discovery of brain permeable 2-Azabicyclo[2.2.2]octane sulfonamides as a novel class of presenilin-1 selective γ -secretase inhibitors



Introduction:

γ -Secretases are membrane bound protease complexes comprising four essential proteins: presenilin (PSEN)¹⁻⁴, nicastrin (NCT), anterior pharynx defective 1 (APH1), and presenilin enhancer 2 (PEN-2).^{4, 5} PSEN is the enzymatic part of the complex hosting two aspartic acid residues D257 and D385 in the transmembrane domain 6 and 7, respectively, forming the catalytic core essential for $A\beta$ generation.^{6, 7} There are two different PSEN isoforms: presenilin-1 (PSEN1) and presenilin-2 (PSEN2) encoded by separate genes in humans.⁵ Likewise, APH1 is also encoded by two different genes, APH1A and APH1B. Altogether there are at least four major γ -secretase complexes: PSEN1-APH1A, PSEN1-APH1B, PSEN2-APH1A and PSEN2-APH1B and having different functions.⁸ Significant heterogeneity exists in the isoforms of PSEN and APH1: PSEN1 and PSEN2 show 65% sequence identity, whereas APH1A and APH1B show 56% identity.⁹ A PSEN1 or APH1A knock out is lethal, and mice die during embryogenesis due to impaired Notch signaling, whereas PSEN2 and APH1B knock out mice display a normal phenotype with no gross abnormalities in fertility, survival, or anatomy.⁹ PSEN1 type γ -secretase complexes seem to produce more $A\beta$ in the brain, whereas PSEN2 type complexes have a smaller contribution.

The main pathological hallmarks of AD are the intracellular neurofibrillary tangles and extracellular deposits of aggregated amyloid β ($A\beta$) peptides. Accumulation of amyloid plaques is thought to trigger cellular response including alterations in microglia, astroglia, and vasculature, leading to the damage and death of neurons, ultimately progressing to dementia.^{10, 11, 12, 13} The decisive processing of APP C-terminal fragment (C-99) is performed by γ -secretase to release C-terminal $A\beta$ peptides. This cleavage is mediated by presenilin, as first demonstrated by De Strooper et al¹⁴ (1998) and confirmed later.^{6, 15, 16} The intramembrane cleavage by γ -secretase results in $A\beta$ fragments of different lengths, predominantly $A\beta_{40}$, along with the more neurotoxic and aggregation prone $A\beta_{42}$ or $A\beta_{43}$ and may even include longer

A β forms in the brain.¹⁷⁻¹⁹ The longer A β species act as seeds leading to the formation of neurotoxic oligomers in the brain, resulting in neuronal dysfunction,^{12, 20} and amyloid fibrils that activate microglia and other cells in AD patients.¹³

The failure of semagacestat, a broad spectrum GSI in Phase III clinical trial emphasizes that broad-spectrum inhibition of all γ -secretases is not a therapeutic option in AD⁸. One of the major problems with full inhibition of γ -secretases is the crucial role it plays in Notch signaling.^{14, 16, 21} Blocking Notch signaling with γ -secretase inhibitors even for a short timespans results in severe problems in skin, blood, and intestine²². Specific inactivation of APH1B γ -secretase in a mouse AD model, on the other hand, results in improvements of AD-relevant phenotypic features without any Notch-related side effects.⁹

While Notch inhibition should be avoided in AD, specific Notch inhibition may have therapeutic value in oncology. Notch signalling has been known to be involved in many aspects of cancer biology, including angiogenesis, tumour immunity, and the maintenance of cancer stem- like cells.²³⁻²⁵ Notch can also act as an oncogene and a tumour suppressor in different cancers and cell populations within the same tumour. PSEN1 and PSEN2 are expressed during human T cell development, and PSEN1 has about 4-fold higher expression compared to PSEN2. However, PSEN1 expression is >30-fold higher than PSEN2 expression in T-ALL cell lines and primary T-ALL patients.²⁴ Given the high frequency of activating Notch1 mutations in cancers, especially in T-ALL, the inhibition of the PSEN1 selective γ -secretase complex provides a potential therapeutic strategy to block the ligand-independent release of notch intracellular domain (NICD).

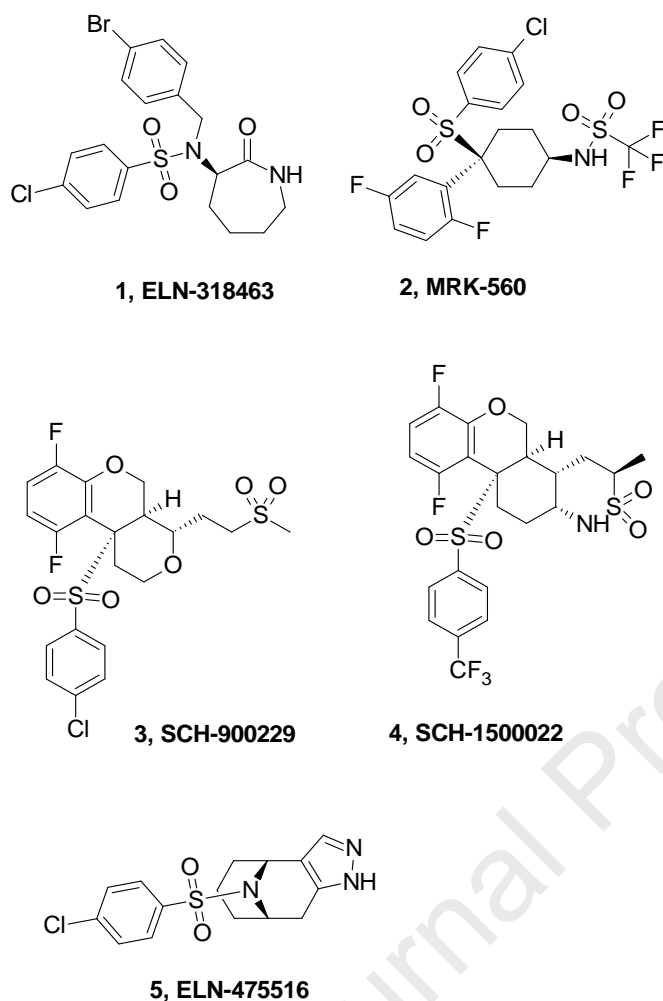
Chronic dosing of **MRK-560 (2)** in mice did not cause Notch related side effects when compared with the other known GSIs, although it does not show selectivity between inhibition of APP and Notch processing in vitro.²⁶⁻²⁸ Later, Zhang et al. found that **MRK-560** and another GSI **SCH-1500022 (4, Figure 1)** display moderate to high selectivity towards the PSEN1

complex (37 and 250-fold, respectively) versus PSEN2 complexes.²⁹ These exceptional and differential effects of **MRK-560** on Notch and APP processing were further explored *in vitro* and *in vivo* by Borgegard et al.³⁰ **MRK-560** potently and dose dependently reduced A β levels in wild type (WT) and PSEN2 deficient mice. While **MRK-560** treatment in wild type mice was safe, mice genetically deficient for PSEN2 suffered from major Notch related toxicity.

Recently, Habets et al. demonstrated that genetic deletion or pharmacologic inhibition of the PSEN1 is highly effective in decreasing leukemia while avoiding dose-limiting toxicities. Clinically, T-ALL samples were found to selectively express only PSEN1-containing γ -secretase complexes. Treatment of T-ALL cell lines with the selective PSEN1 inhibitor **MRK-560** effectively decreased mutant Notch1 processing and led to cell cycle arrest. Moreover, **MRK-560** treatment decreased leukemia burden and increased overall survival without any associated gut toxicity in T-ALL in patient-derived xenografts mice.

These in-vivo proof of concept studies indicate that PSEN2 can take over Notch processing in peripheral organs for a large part when PSEN1 is pharmacologically inhibited and provide a strong hypothesis that sparing PSEN2 inhibition may be a sound strategy towards safe and efficacious GSIs. Although targeting selectively PSEN1-APH1B versus PSEN1-APH1A may also be advantageous, targeting APH1 complexes is pharmacologically not yet viable. Most of the known GSIs are believed to interact with PSEN and currently, there are no reported compounds that significantly discriminate between PSEN1-APH1A and PSEN1-APH1B complexes.

This paper describes the rational design and synthesis of aza-bicyclo-octane sulfonamides as PSEN1 specific inhibitors. We derived structural information and key pharmacophoric features that determine PSEN1 selectivity and developed a series of active compounds that demonstrated low nanomolar potency towards PSEN1-APH1B complex and high selectivity versus PSEN2 complexes.

Figure 1. Chemical structures of known PSEN1 selective γ -secretase inhibitors.

At the time of our exploration, no inhibitor bound structure of γ -secretase was available. Therefore, we considered ligand-based approaches and compared the structures of the known PSEN1 selective molecules to elucidate common structural features required for potency and PSEN1 selectivity. **Figure 1** depicts the examples of PSEN1 selective GSIs reported in the literature. None of the known PSEN1 selective inhibitor was specifically/rationally designed; rather, their attractive PSEN1 complex selectivity was found by serendipity. Carbocyclic sulfone-based **MRK-560 (2)** is described in the literature as a PSEN1 selective inhibitor with moderate selectivity (37-fold) over PSEN2 complexes.²⁹ The Fused bicyclic **SCH-900229 (3)**³¹ has been reported as a PSEN1 selective GSI with 25-fold selectivity, whereas **SCH-1500022**

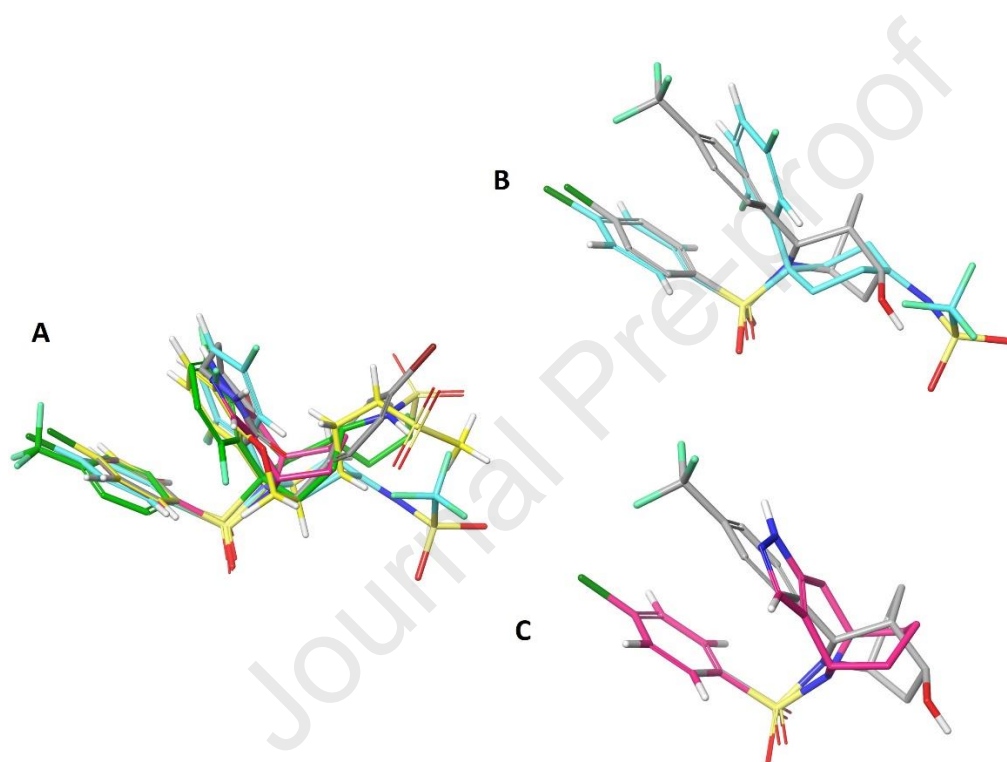
(**4**)²⁹ has been reported as 250-fold selective towards PSEN1 with low nanomolar potency. **ELN-318463** (**1**) was reported as a Notch sparing and PSEN1 selective GSI whereas **ELN-475516** (**5**) as Notch sparing GSI.^{31, 32}

In our hands, **MRK-560** (**2**) displayed sub-nanomolar potency towards PSEN1-APH1B (0.42 nM) and high selectivity versus PSEN-2 complexes (>300 fold). **ELN-318463** (**1**) displayed 24.5 nM potency towards PSEN1-APH1B and >60-fold selectivity versus PSEN2 complexes. Interestingly, conformationally rigid **ELN-475516** (**5**) displayed 10.3 nM potency towards PSEN1-APH1B and high selectivity (>260-fold) selectivity versus PSEN2 complexes.

Small molecule X-ray crystal structures of **MRK-560** analog³³ **SCH-900229** analog³⁴, and **ELN-475516**³⁵ reveal a unique “U” conformation between 4-chlorophenyl sulfone/sulfonamide and 2,5-fluorophenyl/pyrazole moieties. Although, ligand X-ray conformation may not reflect the bioactive conformation, it likely captures a low energy conformation, which is particularly favorable given the relative lack of conformational freedom of these molecules.

To identify and understand the common pharmacophoric features of the known PSEN1 selective inhibitors, **ELN-318463**, **ELN-475516**, **SCH-900229**, **SCH-1500022**, and **MRK-560** were aligned to the reference crystal structure of **ELN-475516** (CCDC 764935) using the Schrodinger’s flexible ligand alignment tool available through the Maestro platform (Schrödinger Release 2023-1: Maestro, Schrödinger, LLC, New York, NY, 2021). All the known selective inhibitors were flexibly aligned on the X-ray reference based on their maximum common substructure (MCS). The overlay of the ligands superposes the common aryl-sulfone or sulfonamide motif that is present in all the molecules, as depicted **Figure 2A-C**. The molecules adopt a “U” conformation where two of the aromatic rings (one from aryl part and other from sulfone/sulfonamide part) of each molecule form intramolecular stacking interactions. The sulfone and sulfonamide aromatic ring are often substituted with similar small

hydrophobic groups such as Cl and CF₃ in the para position, while the other aryl ring tolerates more structural variations. The third branch of the molecules is the carbocyclic core and contains more structural diversity. Usually, in the carbocyclic core of the molecule, a saturated cycle, bicycle or a bridged carbocycle can be allowed. Further substituents in this branch can include more polar groups such as amide carboxylic acid, urea, carbamate, sulfone, or sulfonamides, usually with a H-bond donor, as shown in **Figure 2A**.



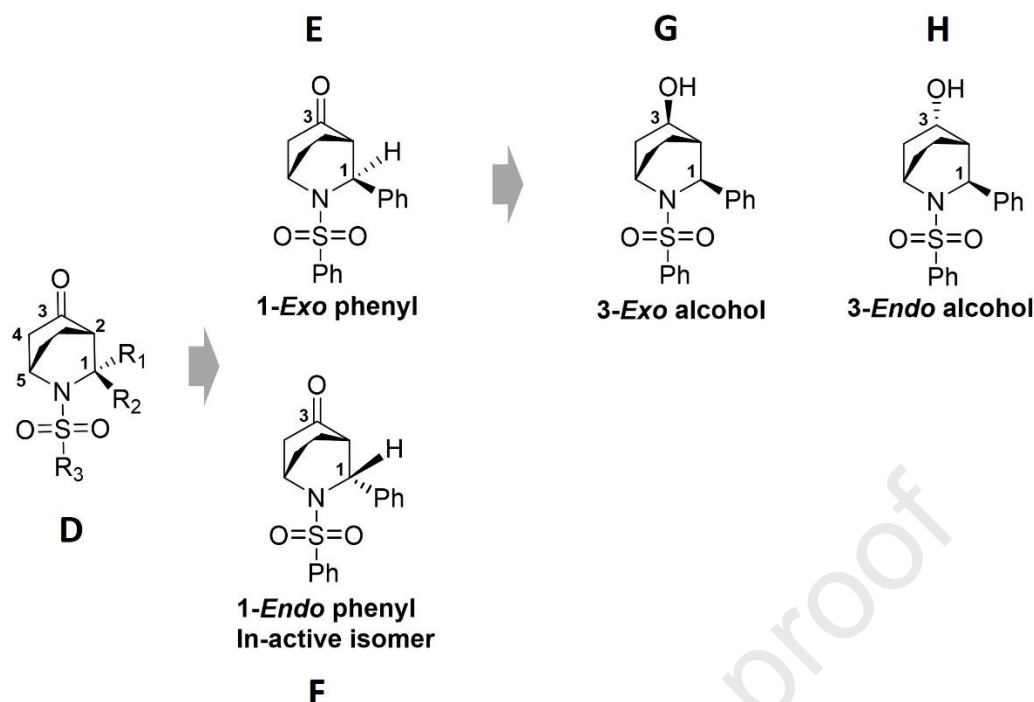


Figure 2. Overlay of **ELN-318463**, **ELN-475516**, **SCH-900229**, **SCH-1500022** and **MRK-560**.³⁶ **A)** Flexible alignment of known GSI using as reference the crystal structure of compound **ELN318463** (CCDC 764935). **B)** Overlay of the designed inhibitor (in grey, **H**) with **MRK-560**. **C)** Overlay of the designed inhibitor (in grey) with **ELN-475516**. **D-F)** Possible isomers of bicyclo-octane scaffold obtained during the synthesis and tested.

The molecular modeling revealed the common 3D conformation for the complex selective inhibitors. Learning from these observations, we explored several bicyclic and tricyclic amine scaffolds that could deliver the same desired 3D arrangement of functional groups. After careful consideration, we shortlisted the [2,2,2] aza-bicyclooctanone scaffold depicted in **Figure 2D** as a preferred cyclic core that would be substituted with aryl and aryl sulfonamide groups to provide the crucial “U” conformation. Any aryl substitution at position “1” of the bicyclic core results in *endo* and *exo* isomers (**Figure 2E-F**).³⁶ Computational modeling studies suggested that the *exo* isomer would provide us the desired “U” conformation between the 4-chlorophenyl sulfonamide and 4-trifluoromethyl phenyl moieties, as depicted in **Figure 2B-C**. Moreover, the ketone group at position “3” of the bicyclic core could be used as a handle to install the various functionalities to understand their impact on potency and selectivity.

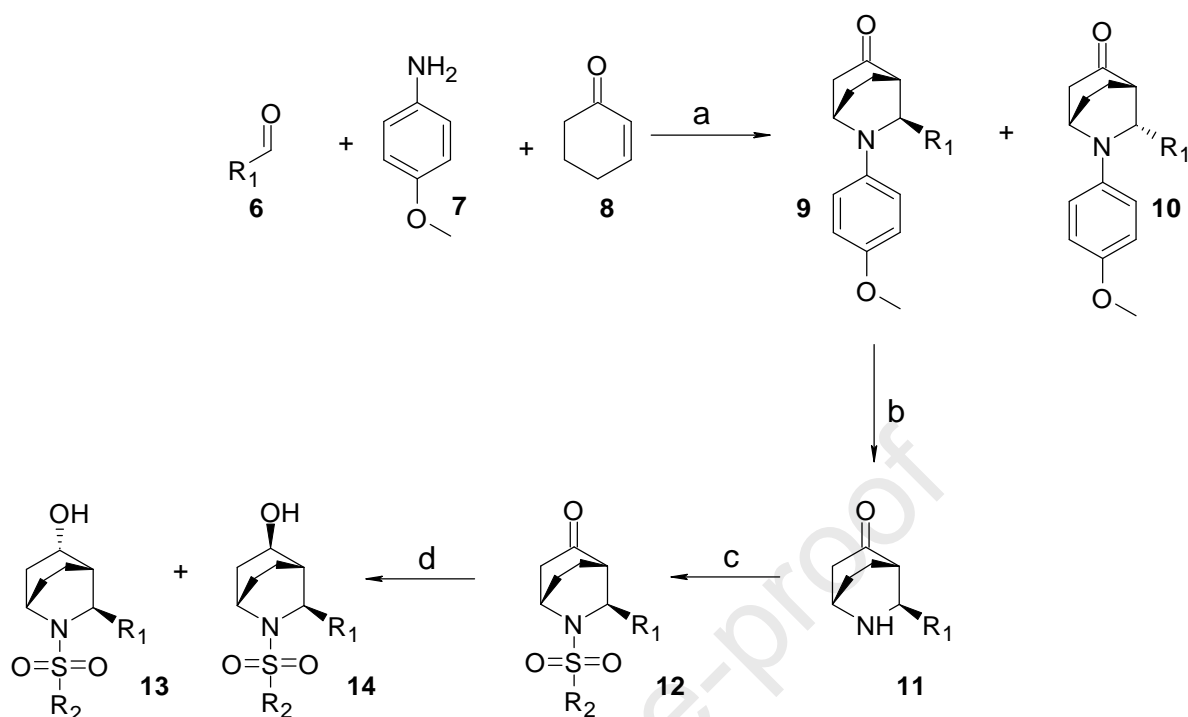
Chemistry

A series of 2-azabicyclo[2.2.2]octane sulfonamides was synthesized as depicted in **Scheme 1**. An equimolar mixture of commercially available aldehydes **6**, *p*-anisidine **7**, 2-cyclohexen-1-one **8** and catalytic bismuth nitrate pentahydrate ($\text{Bi}(\text{NO}_3)_3 \cdot 5\text{H}_2\text{O}$) in anhydrous DMF was heated to 60 °C under microwave conditions to afford the *endo* **9** and *exo* **10** diastereomers with good to moderate yields. Both diastereomers were separated by flash column chromatography. Several catalysts such as InCl_3 , NFSI were employed for the Aza-Diels alder (4+2) cyclization but $\text{Bi}(\text{NO}_3)_3 \cdot 5\text{H}_2\text{O}$ provided the best results in terms of *endo/exo* selectivity, reaction time and yield.³⁷ Several reagents were explored for the 4-methoxy phenyl (PMP) deprotections of **10** such as *N*-bromosuccinimide (NBS), *N*-chlorosuccinimide (NCS), *N*-iodosuccinimide (NIS), and trichloroisocyanuric acid (TCCA).³⁸ Unfortunately, the reaction either did not work or resulted in a complex mixture. Finally, PMP deprotection of **10** was achieved with cerium (IV) ammonium nitrate (CAN) at 0 °C in moderate to low yields to afford amine **11**. *N*-sulfonylation of **11** was achieved using sulfonyl chloride and diisopropyl ethyl amine (DIPEA) in anhydrous dichloromethane (DCM) to provide ketone sulfonamides **12**. Sodium borohydride was employed for the ketone reduction of **12** to afford the the 3-*endo* **13** and 3-*exo* **14** hydroxy isomers.

6-Cyano pyridyl derivative was synthesized as outlined in **Scheme 2**. An equimolar mixture of 6-bromo-3-pyridinecarboxaldehyde **15**, *p*-anisidine **7**, 2-cyclohexen-1-one **8** and catalytic $\text{Bi}(\text{NO}_3)_3 \cdot 5\text{H}_2\text{O}$ in anhydrous DMF was heated to 60 °C under microwave conditions to afford the *exo* **16** and *endo* **17** diastereomers. PMP deprotection of *exo*-isomer **16** was performed with CAN to afford the amine **18** with moderate yield. *N*-sulfonylation of **18** was achieved with sulfonyl chloride and DIPEA in anhydrous DCM to yield the sulfonamide **19**. Ketone reduction with sodium borohydride provided the diastereomeric mixture of alcohol **20**. Cyanation of **20**

was carried out with Zn(CN)_2 and catalytic $(\text{Ph}_3\text{P})_4\text{Pd}$ in DMF at 150 °C under microwave conditions to provide the desired *exo* **21** and *endo* **22** isomers.

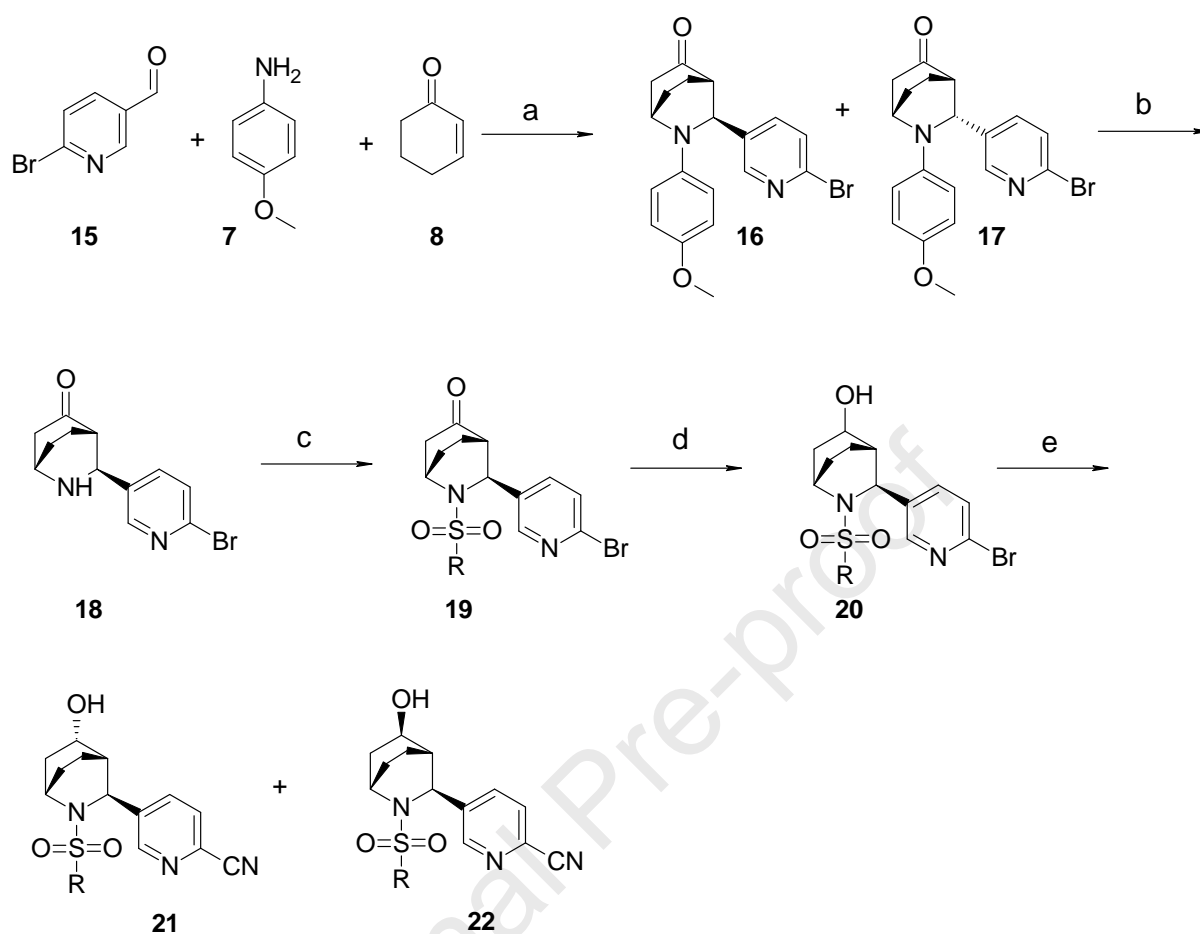
Anilide derivatives **31** were prepared as described in **Scheme 3**. Starting from 4-nitrobenzaldehyde, nitro-substituted **27** was prepared analogous to the reaction sequence described above for compounds **12** (as in **Scheme 1**). Chemo-selective nitro group reduction of **27** was achieved with anhydrous SnCl_2 in absolute ethanol at 75 °C to give aniline **28**. *N*-acylation of **28a-b** was carried out using acid chloride and DIPEA in DCM to afford the acetamide derivatives **29a-c**. Aniline **28** was treated with ethyl chloroformate and DIPEA in DCM to afford the carbamate derivative **29d**. Urea derivative **29e** was synthesized by treating aniline **28** with ethyl isocyanate and DIPEA in DCM. Ketone reduction of **29** was accomplished using sodium borohydride in methanol to generate the desired 3-*exo* **30** and 3-*endo* **31** isomers

Scheme 1. General Synthetic scheme for bicyclooctane sulfonamides^a

Compound	R ₁	R ₂
12a, 13a, 14a	2,5-difluoro phenyl	4-chloro phenyl
12b, 13b, 14b	4-trifluoromethyl phenyl	4-chloro phenyl
12c, 13c, 14c	2-chloro phenyl	4-chloro phenyl
12d, 13d, 14d	6-trifluoromethyl pyridyl	4-chloro phenyl
12e, 13e, 14e	6-methoxy pyridyl	4-chloro phenyl
12f, 13f, 14f	4-chloro phenyl	4-chloro phenyl
12g, 13g, 14g	3,4-difluoro phenyl	4-chloro phenyl
12h, 13h, 14h	4-cyano phenyl	4-chloro phenyl
12i, 13i, 14i	Phenyl	4-chloro phenyl
12j, 13j, 14j	4-trifluoromethoxy phenyl	4-chloro phenyl
12k, 13k, 14k	2-fluoro-4-cyano phenyl	4-chloro phenyl
12l, 13l, 14l	4-chloro phenyl	5-Chloro thiophenyl
12m, 13m, 14m	3,4-difluoro phenyl	5-Chloro thiophenyl

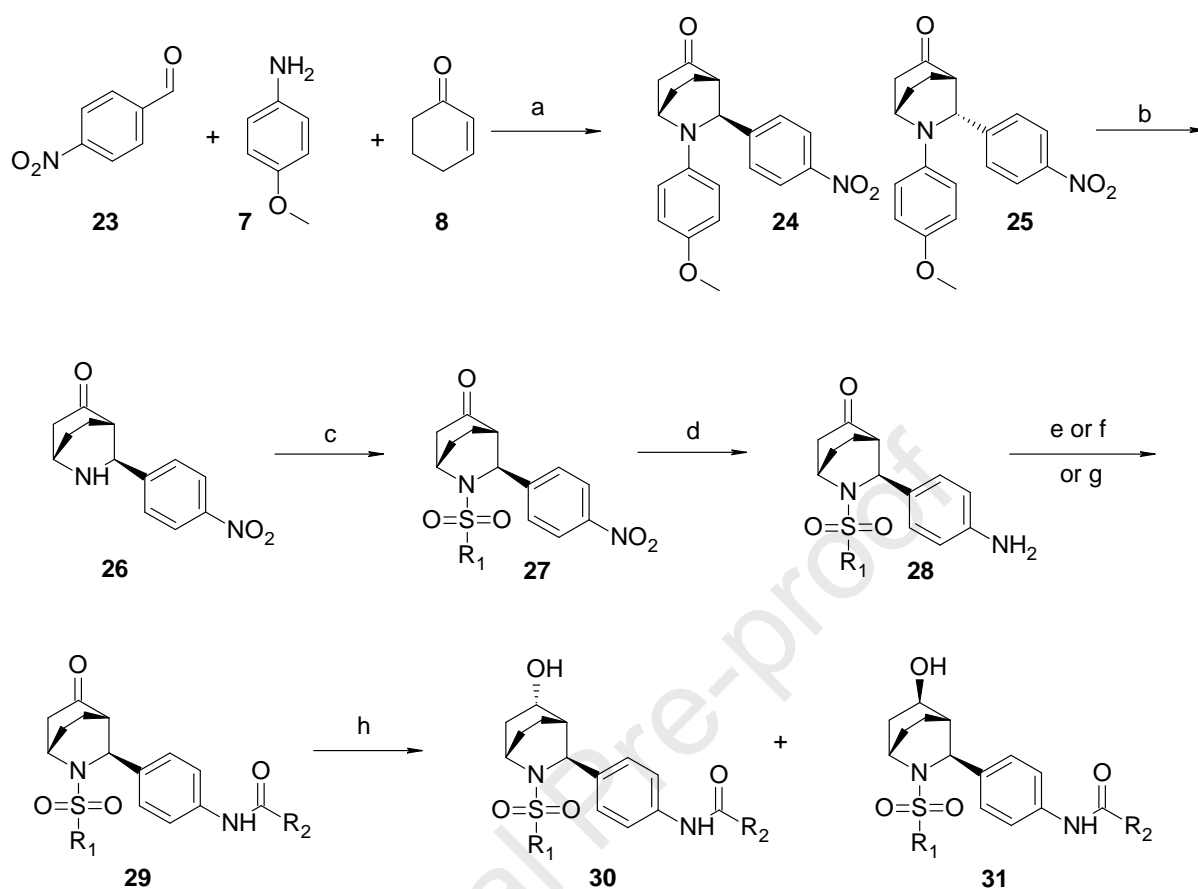
12n, 13n, 14n	4-trifluoromethyl phenyl	4-methyl phenyl
12o, 13o, 14o	3,4-difluoro phenyl	5-Chloro thiophenyl
12p, 13p, 14p	3,4-difluoro phenyl	5-Chloro thiophenyl

“Reagents and conditions: (a) $\text{Bi}(\text{NO}_3)_3 \cdot 5\text{H}_2\text{O}$, DMF, 60 °C, microwave, 2 h, 30-60%; (b) $(\text{NH}_4)_2\text{Ce}(\text{NO}_3)_6$, $\text{H}_2\text{O}:\text{CH}_3\text{CN}$ (1:1), 0 °C, 1 h, 30–70%; (c) $\text{R}_2\text{SO}_2\text{Cl}$, DIPEA, CH_2Cl_2 , 0 °C, 2 -18 h, 40–80%; (d) NaBH_4 , MeOH, RT, 2–18 h, 80-95%.

Scheme 2. Synthesis 6-cyano pyridyl derivatives^a

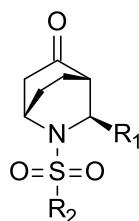
Compound	R ₂
20a, 21a, 22a	4-chlorophenyl
20b, 21b, 22b	5-Chlorothiophenyl
20c, 21c, 22c	4-methylphenyl

“Reagents and conditions: (a) $Bi(NO_3)_3 \cdot 5H_2O$, DMF, 60 °C, microwave, 2 h, 60%; (b) $(NH_4)_2Ce(NO_3)_6$, $H_2O:CH_3CN$ (1:1), 0 °C, 1 h, 30–70%; (c) R_2SO_2Cl , DIPEA, CH_2Cl_2 , 0 °C, 2–18 h, 40–80%; (d) $NaBH_4$, MeOH, RT, 2–18 h, 80–95%; (e) $Zn(CN)_2$, $(PPh_3)_4Pd$, DMF, 160 °C, microwave, 10 min, 74%.

Scheme 3. Synthesis *p*-substituted derivatives^a

Compound	R_1	R_2
29a, 30a, 31a	4-chlorophenyl	CH_3
29b, 30b, 31b	5-Chlorothiophenyl	CH_3
29c, 30c, 31c	4-chlorophenyl	CH_2OCH_3
29d, 30d, 31d	4-chlorophenyl	OCH_2CH_3
29e, 30e, 31e	4-chlorophenyl	$NHCH_2CH_3$

^aReagents and conditions: (a) $Bi(NO_3)_3 \cdot 5H_2O$, DMF, 60 °C, microwave, 2 h, 60%; (b) $(NH_4)_2Ce(NO_3)_6$, $H_2O:CH_3CN$ (1:1), 0 °C, 1 h, 55%; (c) R_1SO_2Cl , DIPEA, CH_2Cl_2 , 0 °C to RT, 2 -18 h, 50–70%; (d) anhydrous $SnCl_2$, abs. ethanol, reflux, 4 h, 60%, (e) R_2COCl , DIPEA, CH_2Cl_2 , 0 °C to RT, 4 h, 60–65%; (f) ethyl chloroformate, DIPEA, CH_2Cl_2 , 0 °C, 18 h, 73%; (g) ethyl isocyanate, DIPEA, CH_2Cl_2 , 0 °C to RT, 18 h, 80%; (h) $NaBH_4$, MeOH, RT, 2 h, 80–95%;

Table 2. Activity Data for Racemic *Exo*-Ketones

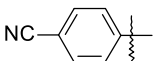
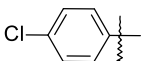
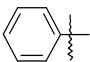
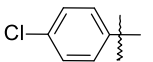
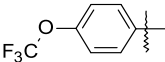
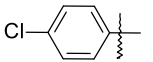
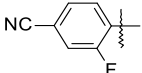
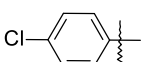
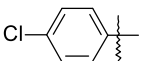
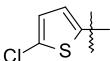
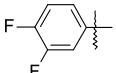
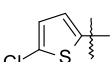
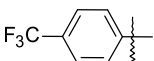
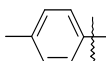
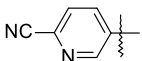
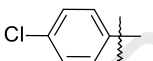
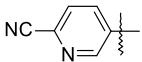
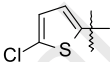
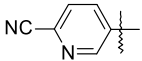

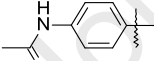
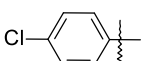
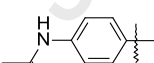
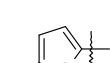
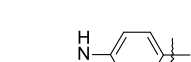
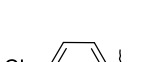
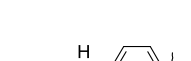

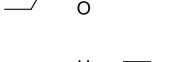

Entry	Compd	R ₁	R ₂	IC ₅₀ (nM) ^a			
				PSEN1- APH1A	PSEN1- APH1B	PSEN2- APH1A	PSEN2- APH1B
1	12a			1023	426	>10000	>10000
2	12b			316	34	>10000	>5000
3	12c			2630	389	>10000	>10000
4	12d			690	390	>10000	>10000
5	12e			794	195	>10000	>10000
6	12f			1349	182	>10000	>10000
7	12g			>5370	1120	>10000	>10000
8	12h			891	234	>8000	>8000
9	12j			1621	190	>10000	>10000
10	12k			691	131	3388	7585
11	12l			2238	281	>10000	>10000

12	12m			>10000	1949	>10000	>10000
13	12n			7079	512	>10000	>10000
14	12o			1905	588	>10000	>10000
15	12p			281	55	>5000	>5000
16	12q			1000	208	>10000	>10000
17	12r			>10000	1548	>10000	>10000
18	12s			>10000	1445	>10000	>10000
19	12t			>10000	5888	>10000	>10000
20	29a			6309	709	>10000	>10000
21	29b			3020	389	8500	8000
22	29c			>10000	1445	>10000	>10000
23	29d			3235	288	6166	6456
24	29e			3801	389	7000	8500

^aThe IC₅₀ values for the various complexes represent the mean values of at least two independent experiments.

Table 3. Activity Data for racemic **3-Exo** and **3-Endo** Alcohols

Entry	Compd	R ₁	R ₂	-OH Endo/ Exo	IC ₅₀ (nM) ^a			
					PSEN1- APH1A	PSEN1- APH1B	PSEN2- APH1A	PSEN2- APH1B
1	13a			<i>Endo</i>	37	25	370	380
2	14a			<i>Exo</i>	851	427	7760	7759
3	13b			<i>Endo</i>	41.7	7.2	2818	2454
4	14b			<i>Exo</i>	758	109	>10000	>10000
5	13c			<i>Endo</i>	12	3	131	214
6	14c			<i>Exo</i>	2238	426	>10000	>10000
7	13d			<i>Endo</i>	263	38	>2000	>2000
8	14d			<i>Exo</i>	6456	776	>10000	>10000
9	13e			<i>Endo</i>	380	62	>10000	>10000
10	13f			<i>Endo</i>	147	46	>2000	>2000
11	13g			<i>Endo</i>	295	58	>10000	>10000

12	13h			<i>Endo</i>	64	12	758	631
13	13i			<i>Endo</i>	102	14	426	602
14	13j			<i>Endo</i>	151	37	>10000	>10000
15	13k			<i>Endo</i>	6.9	2.4	147	257
16	13l			<i>Endo</i>	199	58	>2000	>2000
17	13m			<i>Endo</i>	398	74	>10000	>10000
18	13n			<i>Endo</i>	208	50	>8000	>8000
19	21a			<i>Endo</i>	67	12	741	2178
20	21b			<i>Endo</i>	147	39	3020	3388
21	21c			<i>Endo</i>	1096	158	>10000	>10000
22	30a			<i>Endo</i>	135	24.5	1200	>1300
23	30b			<i>Endo</i>	72.4	26	513	851
24	30c			<i>Endo</i>	208	52	1412	1995
25	30d			<i>Endo</i>	190	29	288	912
26	30e			<i>Endo</i>	446	79.4	2344	4786
27	1, ELN-318463				38.3	24.5	4113	1705

28	2, MRK-560	1.4	0.42	153.5	139.4
29	5, ELN-475516	47.2	10.3	272.4	380.3

^aThe IC₅₀ values for the various complexes represent the mean values of at least two independent experiments.

Results and Discussion:

Recently we reported a novel cellular assay to measure the activity of the four individual γ -secretase complexes.³⁶ Mouse Embryonic Fibroblast (MEF) cells deficient for the *Psen* and *Aph1* genes (*Psen1/2*^{-/-}, *Aph1ABC*^{-/-}) were reconstituted with human PSEN1 or PSEN2 and with human APH1A or APH1B to generate four independent cell lines, each constitutively expressing exclusively one type of γ -secretase complex. All newly synthesized compounds were tested in our sandwich ELISA assay for their inhibitory activity towards the four γ -secretase complexes: PSEN1-APH1A, PSEN1-APH1B, PSEN2-APH1A and PSEN2-APH1B (Tables 2-3). To begin with, we chose 2,5-difluoro phenyl substituent at position “1” of the bicyclic core as a model substituent taking a clue from the **MRK-560** series of compounds. First, the racemic intermediates *exo* **9a** and *endo* **10a** were tested for their ability to inhibit the γ -secretase complexes to investigate the importance of the aryl sulfonamide group. Both these compounds possess an *N*-4-methoxy phenyl group instead of the required *N*-aryl sulfonyl. As expected, *exo* **9a** and *endo* **10a** did not show any inhibition at 30 μ M concentration. Next, we synthesized and tested racemic *exo* bicyclo-octanone sulfonamide derivatives **12a** and its *endo* analog. Gratifyingly, **12a** displayed moderate inhibitory activity towards PSEN1-APH1B complex with IC₅₀ of 426 nM, and at least 25-fold selectivity versus PSEN2 complexes. In comparison, the *endo* analog of **12a** displayed very weak inhibitory activity towards PSEN1-APH1B (45% inhibition at 10 μ M; data not shown). This was routinely the case with the *endo* analogs therefore further work was only targeted to the *exo* analogs.

Encouraged by these results, a series of racemic analogs **12b-p** and **29a-e** was synthesized and tested. Substituents at position “1” of the bicyclic core were chosen based on the SAR from the previously known GSIs and keeping in mind the effect of substituents on the physicochemical properties such as lipophilicity and polar surface area. 4-Chlorophenyl sulfonyl and 2-chlorothiophenyl sulfonyl were chosen as preferred substituents representing the aryl sulfonyls from literature data.

All the compounds displayed good to high selectivity towards PSEN1 complexes (PSEN1-APH1A, PSEN1-APH1B) compared to the PSEN2 complexes (PSEN2-APH1A, PSEN2-APH1B). None of the compound displayed 100% inhibition versus PSEN2 complexes even at the highest concentration (10 μ M). All the compounds displayed highest potency towards PSEN1-APH1B ranging from 34 to 1949 nM. **12b** turned out to be the most potent of all the tested ketones: 34 nM potency towards PSEN1-APH1B, 9-fold selectivity towards PSEN1-APH1A (316 nM), and >150-fold selectivity towards both PSEN2 complexes. Modifying the 2,5-difluoro position of **12a** to 3,4-difluoro in **12g** resulted in a >3-fold loss in potency (1120 nM) towards PSEN1-APH1B complex. Changing the -CF₃ of **12b** to its bio-isosteric equivalents -Cl as in **12f** and -OCF₃ as in **12j** caused in a >5-fold loss of potency (IC₅₀ = 182 and 190 nM for PSEN1-APH1B complex, respectively). Replacing 4-trifluoromethyl phenyl as in **12b** to 4-trifluoro pyridyl **12d** resulted in significant loss of potency (>11 fold; 390 nM) towards PSEN1-APH1B complex whereas methoxy pyridyl **12e** replacement decreased potency by >5 fold (195 nM). Ortho substituted phenyl at position “1” of the bicyclic core did not improve the potency and selectivity towards PSEN1-APH1B complex compared to **12b**. 2-Chloro phenyl **12c** and 2-F, 4-CN phenyl **12k** were 11 and 4-fold less potent compared to **12b**, respectively. Compounds **12l-o** were synthesized to probe the effect of 2-chlorothiophenyl sulfonyl towards potency and selectivity. Introduction of 2-chlorothiophenyl as a bio-isosteric

replacement of 4-chloro phenyl resulted in slight decrease in potency towards PSEN1-APH1B complex in general while retaining the selectivity versus PSEN2 complexes.

Compounds **29a-e** were synthesized to investigate the effect of hydrophilic substituents at para position and compared with **12b** in terms of potency and selectivity. Introduction of hydrophilic substituents such as acetamide, carbamate, and urea as detailed in **29a-e** improved the physicochemical properties such as cLogP and solubility but the potency towards PSEN1-APH1B complex was significantly decreased, especially in **29c** when compared to **12b**. Carbamate derivative **29d** turned out as the most potent compound of the series **29a-e** with IC₅₀ of 288 nM for PSEN1-APH1B complex, 11-fold selectivity versus PSEN1-APH1A complex, and more than 20-fold selectivity compared to PSEN2 complexes.

Since **12b** was the most potent compound in the series, we decided to explore the substituents on the sulfonyl phenyl without altering the trifluoromethyl phenyl group at position “1” of the bicyclic core. Accordingly, we synthesized a small set of compounds **12p-t** where we replaced the 4-Cl phenyl with 4-Me, 4-F, 4-CN, 4-OMe, and 2-Cl phenyl. Next, compounds **12p-t** were screened to probe their inhibitory activity against γ -secretase complexes. Compound **12p** displayed high potency (55 nM) towards PSEN1-APH1B complex and >100-fold selectivity versus PSEN2 complexes. Introduction of 4-F in **12q** was tolerated, but decreased the potency by >6-fold towards PSEN1-APH1B complex when compared to **12b**. Replacement by hydrophilic/polar substituents such as -OMe and -CN (**12 r-s**) resulted in significant loss of potency (>40-fold) towards PSEN1 complexes. Shifting the position of 4-Cl in **12b** to 2-Cl as in **12t** proved detrimental and resulted in complete loss of potency towards all four complexes. To summarize the structure activity relationship (SAR) data for ketones (**Table 2**): **12b** turned out to be the most potent compound with low nanomolar potency towards PSEN1-APH1B and high selectivity versus PSEN2-complexes. Hydrophilic/polar substituents at the 4-position of phenyl sulfonamides were detrimental for potency and so was placing Cl group to the 2-

position of phenyl sulfonamide. Replacing a 4-Cl phenyl sulfonamide with 4-Me and 4-F phenyl sulfonamide was tolerated with slight decrease (1.5 to 8-folds) in potency whereas introducing 5-Cl thiophene sulfonamide maintained the potency.

Most of the PSEN1 complex selective GSIs harbor the H-bond donor in their scaffolds usually as a -NH either from a sulfonamide or an amide functionality. Literature data suggests that in most cases, having such hydrogen bond donors is not required for the primary activity, but crucial for physicochemical properties, and bioavailability.²⁶ SAR data from **ELN475516** shows that the hydrogen bond donor (-NH) on the pyrazole group is vital for potency and any modification of the pyrazole results in complete loss of potency, (**Figure 1**).³⁵ Considering the effect of the hydrogen bond donors, -OH functional group was introduced by simply reducing the ketone of **12**, **19** and **29**. Reduction of ketone provided 3-*exo* (**13**, **21** and **30**) and 3-*endo* (**14**, **22** and **31**) diastereomers which were separated by preparative HPLC. Subsequently, alcohols **13**, **14**, **20**, **21**, **30**, and **31** were investigated for their ability to inhibit γ -secretase complexes. Introducing the -OH group significantly enhanced the potency towards PSEN1 complexes while maintaining the selectivity versus PSEN2 complexes. In general, *endo* alcohols were substantially more potent towards PSEN1-APH1B complex than their corresponding *exo* alcohols (up to 140-fold). In most cases, the potency of the *exo* alcohols towards PSEN1-APH1B complex was comparable with their parent ketones indicating that the orientation of -OH group is key for high potency. Of all the tested alcohols, **13c** and **13k** turned out to be the most potent compounds towards PSEN1-APH1B complex with an IC₅₀ of 3 and 2.4 nM respectively, while moderate selectivity versus PSEN2-complex was observed (40 to 60-fold for PSEN2-APH1A and 70 to 100-fold for PSEN2-APH1B). **13a** turned out to be the least selective inhibitor with decent potency towards PSEN1-APH1B (IC₅₀ = 25 nM), while almost no selectivity towards PSEN1-APH1A complex (IC₅₀ = 37 nM) and minor selectivity with PSEN2 complexes (12 to 13-fold). Of all the alcohols tested, **13b** was the standout

inhibitor in terms of potency and selectivity towards PSEN1-APH1B. **13b** displayed high potency towards PSEN1-APH1B ($IC_{50} = 7.2$ nM) with minor selectivity (>5 -fold) towards PSEN1-APH1A complex ($IC_{50} = 41.7$ nM) and high selectivity versus PSEN2-complexes (>390 -fold for PSEN2-APH1A and >330 -fold for PSEN2-APH1B). In general, lipophilic substituents at the para position of the phenyl ring (at position R_1) improved the potency towards PSEN1-APH1B complex and the selectivity versus PSEN2-complexes (as observed in **13b**, **13d**, **13f**, **13g**, **13j**). Conversely, introduction of hydrophilic/polar substituents at the same position retained the potency towards PSEN1-APH1B complex but lost the selectivity versus PSEN2-complexes as observed in **13h**, **21a**, **30a**, **30c**, **30d**, **30e**, **13j**. Exceptionally, compound **13e** bearing a polar/hydrophilic 2-methoxy pyridyl substituent (at position R_1) retained the potency towards PSEN1-APH1B ($IC_{50} = 62$ nM) and selectivity versus PSEN2 complexes. In contrast to what was observed in ketones: incorporation of an ortho substituent of the phenyl ring (at position R_1) significantly boosted the potency towards PSEN1-complexes (as observed in **13a**, **13c**, and **13k**) but lessened the selectivity versus PSEN2 complexes compared to **13b**.

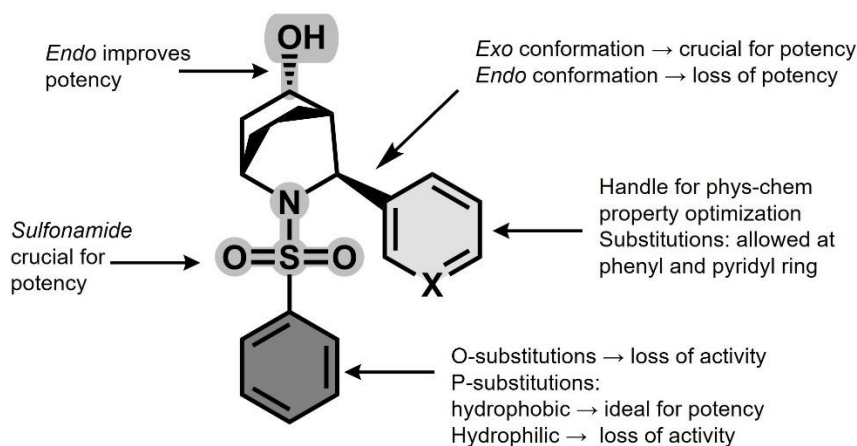
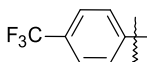
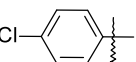
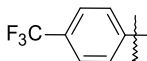
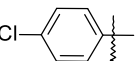
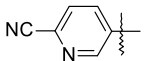
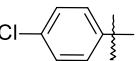
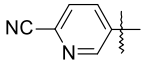
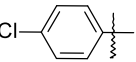


Figure 3. Key structural features required for potency towards PSEN1 complexes.

As observed in ketones (**12** and **29**), 5-chlorothiophene and 4-methyl phenyl sulfonamide containing alcohols conserved potency towards PSEN1-complexes compared to their 4-chlorophenyl sulfonamide analogs. *Endo* 5-chlorothiophene sulfonamide alcohols (as observed in **13l-m**, **12b** and **30b**) were equipotent compared to their *endo* 4-chlorophenyl sulfonamide alcohols. However, replacing 4-chlorophenyl sulfonamides with 4-methylphenyl sulfonamides resulted in 7 to 12-fold drop towards PSEN1-APH1B complex while maintaining selectivity versus PSEN2 complexes. The key structural features required for the potency are summarized in **Figure 3**.

Considering the potency towards PSEN1 complexes, selectivity versus PSEN2 complexes and physicochemical properties (such as cLogP, tPSA), we chose **13b** and **21a** as lead compounds and their enantiomeric separation was performed using chiral supercritical fluid chromatography (SFC) techniques. The activity data for the pure enantiomers is described in **Table 4**.

Table 4. Activity Data for enantiomers of **13b** and **21a**

Compd	R ₁	R ₂	IC ₅₀ (nM)			
			PSEN1-APH1A	PSEN1-APH1B	PSEN2-APH1A	PSEN2-APH1B
(+) 13b			19	5.5	1950	2138
(-) 13b			759	110	>10000	>10000
(+) 21a			72	12.9	1230	776
(-) 21a			>10000	>10000	>10000	>10000

Isomer (+)-**13b** displayed improved potency towards PSEN1-APH1B (**Figure 4**) while maintaining the selectivity versus PSEN2 complexes (>300-fold) while (-)-**13b** displayed 15-fold less potency towards PSEN1-APH1B. Importantly, the residual activity of (-)-**13b** observed towards PSEN1 complexes could be due to the traces of active enantiomer (+)-**13b** (~3%) present. Similarly, (+)-**21a** isomer displayed high potency towards PSEN1-APH1B and selectivity versus PSEN2 complexes, whereas (-)-**21a** turned out to be completely inactive towards PSEN1 and PSEN2 complexes ($IC_{50} = >10000$ nM).

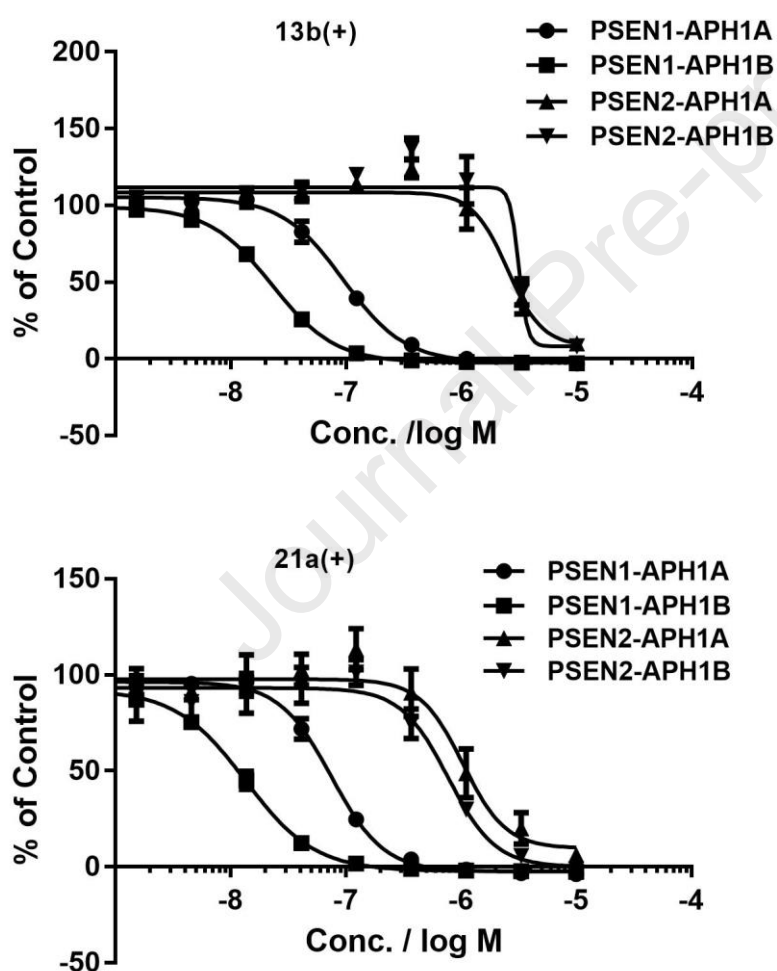


Figure 4. Dose response curve for (+)-**13b** and (+)-**21a**

CYP450 (CYPs) comprises a superfamily of isoforms which play a critical role in the oxidative metabolism of commonly used drugs and several endogenous compounds. We tested a set of *endo* alcohols for their ability to inhibit six major CYP450 isoforms (3A4_M, 2C8, 2C9, 2C19, 2D6, and 1A2) and the data are detailed in the supplementary information, **SI-Table 2**. Significantly, all the compounds displayed very weak inhibition towards 2C8, 2D6, and 1A2 (with $IC_{50} = 10 \mu M$). When tested for 2C19 and 3A4_M inhibitory activity, most of the compounds displayed weak to moderate inhibition with IC_{50} ranging from $1 \mu M$ to $>10 \mu M$. It is important to note that CYP inhibition, especially 2C9 inhibition was reported to be one of the critical issues for MRK-560 and its next generation of PSEN1 selective inhibitors.³⁹

Metabolic stability is a critical factor for the progress of a drug candidate in development apart from its primary biological activity. With the potent and complex selective inhibitors in hand, the metabolic stability of the compounds (as detailed in supplementary information, **SI-Table 2**) was assessed in *in vitro* incubations in the presence of human liver microsomes and mouse liver microsomes and subsequently quantified by liquid chromatography-mass spectrometry (LC-MS). Unfortunately, most of the compounds displayed high clearance in human and mouse liver microsomes. As expected, compounds with higher lipophilicity ($cLogP > 4$) turned out to be the most unstable ones with high clearance ($CL_{int} > 347 \mu L/min/g$). Reducing the lipophilicity significantly improved metabolic stability for some compounds in comparison with **13b**, yet still not in a desirable range (as observed in **13h**, **13k**, **30b**, and **30c**). The lead compound **13b** ($cLogP = 4.64$) demonstrated high clearance ($CL_{int} > 347 \mu L/min/g$) in both human and mouse liver microsomes whereas **21a** ($cLogP = 2.09$) bearing a 2-cyanopyridyl group at R_1 displayed moderate improvement ($CL_{int} = 111$ and $118 \mu L/min/g$ in hLM and mLM respectively).

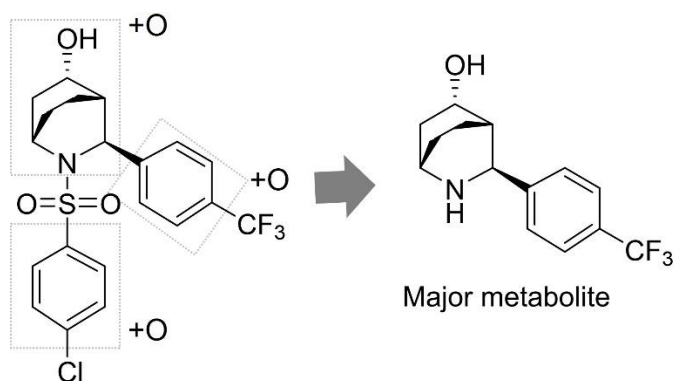


Figure 5. Metabolite identifications studies with (+)-**13b**. Hydrolysis of sulfonamide was identified as major metabolic route.

Metabolite identification (Met-ID) studies were performed with (+)-**13b** to identify the metabolic hotspots. Met-ID studies indicated that hydrolysis of aryl sulfonamide was the major metabolic route along with other minor metabolites as depicted in **Figure 5**. Several bio-isosteric sulfonamide replacements were introduced such as amide, carbamate, and urea to mitigate the high clearance. However, replacement of sulfonamide group resulted in complete loss of activity (supplementary information, compounds **SI-1** to **SI-3**). The loss of potency can be attributed to the fact that bio-isosteric replacements of sulfonamide group do not adopt the “U” shape which we believe is an important factor for potency.

Table 5. *In vitro* profile of (+)-**13b** and (+)-**21a**

Parameter	(+)- 13b	(+)- 21a
cLogP	4.64	2.09
tPSA	57.6	94.3
HLM CL _{int} (μL/min/mg)	>347	78.4
MLM CL _{int} (μL/min/mg)	>347	110
CYP450 Inhibition, IC ₅₀ ((μM))		
3A4 (midazolam)	3	>10
2C8 (Amodiaquine)	>10	>10
2C9 (tolbutamide)	>10	>10

2C19 (S-mephenytoin)	>10	>10
2D6 (dextrometorphan)	>10	>10
1A2 (phenacetin)	>10	>10
Plasma Protein Binding (% free)		
Human	NT	15.6
Mouse	0.309	8.69
Brain Tissue Binding (% free)		
Rat	0.115	11.95
Kinetic Solubility (μM)		
Buffer pH 2.0	13	13
Buffer pH 4.0	12	13
Buffer pH 7.4	18	7
Permeability (LLC-MDR1 Cells)		
Papp (A-B)+Inhibitor (10^{-6} cm/s)	5.6	33.3
Papp (A-B) (10^{-6} cm/s)	6.3	2.5
Papp (B-A) (10^{-6} cm/s)	12.3	79.7
BA/AB ratio	1.95	32.3
Cardiovascular Safety		
hERG binding IC_{50} (μM)	>10	>10
rCaCH binding IC_{50} (μM)	>10	>10
rNaCH binding IC_{50} (μM)	>10	>10

The

lead

compounds (+)-**13b** and (+)-**21a** were evaluated further for their in vitro ADME properties.

The most relevant physicochemical and in vitro data are tabulated in **Table 5**. As already observed for racemates **13b** and **21a**, metabolic stability was poor in both species with a very high turnover in human and mouse microsomes ($\text{CL}_{\text{int}} = >347 \mu\text{L}/\text{min}/\text{g}$) for (+)-**13b** whereas moderate improvement was observed in case of (+)-**21a**. Both compounds displayed weak

inhibitory activity towards cytochrome P450 with IC₅₀ values varying from 3 to >10 μ M for the various isoforms in human liver microsomes. In accordance with relatively higher lipophilicity of (+)-**13b**, over 99% plasma protein binding and brain tissue binding was observed. The lower lipophilicity in (+)-**21a** resulted in significantly lower plasma protein binding and brain tissue. (+)-**13b** and (+)-**21a**, both displayed moderate solubility across pH range. (+)-**13b** displayed a moderate permeability in MDR1-expressing LLC-PK1 cells (LLC-MDR1, 6.3×10^{-6} cm/s) with no indication of P-glycoprotein mediated efflux. A poor permeability was observed with (+)-**21a** (LLC-MDR1, 2.5×10^{-6} cm/s) with a high efflux ratio (>32) indicating that it might be suffer from P-glycoprotein mediated efflux.

In-vivo studies

Despite the high clearance in hLM and mLM, (+)-**13b** and (+)-**21a** were evaluated in vivo. At first, the ability to cross the blood brain barrier (BBB) was investigated. Fed male Swiss mice (n = 3) were dosed (2.5 mg/kg) via iv route and the levels of the compound in brain and plasma were quantified 5 min post dosing. The results are summarized in **Table 6**. Significantly higher brain levels (3623 ± 665 ng/g) of (+)-**13b** were observed compared to plasma (680 ng/mL) resulting in high brain/plasma ratio (5.4). However, due to the very high brain tissue binding, the brain unbound fraction was 2.1 ng/mL which corresponds to 9 nM (1.7 times of IC₅₀). The observed levels of (+)-**21a** in CD1 mice brain were significantly lower than plasma (brain plasma ratio of 0.5) and significantly lower when compared to (+)-**13b**. However, the unbound levels of (+)-**21a** were significantly higher owing to comparatively lower plasma protein binding and brain tissue binding. For brain, the unbound fraction of (+)-**21a** was 43 ng/mL which corresponds to 106 nM (~8 times of IC₅₀).

Upon dosing *p.o.* with 30 mg/Kg to fed CD1 mice, significantly lower levels of (+)-**13b** and (+)-**21a** were observed 4 hours post dosing, in both brain and plasma (data not shown). The high clearance of (+)-**13b** and high efflux ratio (>32) of (+)-**21a** limited us to profile

extensively in mouse models to investigate the pharmacokinetic and pharmacodynamic parameters. Nonetheless, we decided to perform in vivo PK studies with (+)-**13b** to understand the in vivo $T_{1/2}$, distribution, and clearance over 2 h post dose. Fed CD1 male mice ($n = 3$) were dosed (1 mg/kg) via iv route. As expected, the clearance (CL) data are in line with the in vitro prediction: (+)-**13b** displayed very high clearance (99 mL/min/kg) with the mean $T_{1/2}$ of 0.48 h (Table 7). The volume of distribution (V_{dss}), on the other hand was large (3.43 L/kg) which is ~4.73 times higher than total body water indicating that the compound distributed extensively outside plasma.

Table 6. Brain and plasma levels of (+)-13b and (+)-21a at 5 min post dose in male mice^a

Comd	Route	Dose (mg/kg)	Plasma (ng/mL)	Brain (ng/g)	Brain/ Plasma ratio	$f_{u, \text{plasma}}$ (ng/mL)	$f_{u, \text{brain}}$ (ng/g)	$^c K_{p, u, u}$
(+) 13b	iv ^b	2.5	680 ± 144	3623 ± 665	5.4 ± 0.8	2.1	4.14	1.97
(+) 21a	iv ^b	2.5	731 ± 48	363 ± 29	0.5 ± 0.073	63.5	43.3	0.68

^aData represent means ± standard errors of the mean ($n = 3$). ^b Vehicle for iv PEG400:water (70:30). Dose concentration (0.5 mg/mL). ^c $K_{p, u, u}$ (concentration ratio of unbound drug in brain to plasma)

Table 7. Single-Dose Pharmacokinetic Parameters of Compound (+)-13b in male mice^a

Route	Dose (mg/kg)	$T_{1/2}$ (h)	T_{\max} (h)	AUC_{Last} (ng.h/mL)	$AUC_{0-\text{inf}}$ (ng.h/mL)	V_{ss} (L/Kg)	CL (mL/min/kg)	MRT (h)
iv ^b	1	0.481 ± 0.057	2 h	163 ± 28	174 ± 34	3.43 ± 0.58	99 ± 19	0.453 ±0.054

^aData represent means ± standard errors of the mean ($n = 3$). ^b Vehicle for iv PEG400:water (70:30). Dose concentration (0.4 mg/mL)

Genetic and biochemical evidence indicate that compounds targeting PSEN1-APH1B could be of major benefit to the patients. But, achieving significant selectivity between PSEN1-APH1A and PSEN1-APH1B appears unattainable for now. APH1 is not the part of the catalytic subunit and its localization on the active γ -secretase complex is too far away from the active site to create a bias in the catalytic subunit (PSEN1) to drive the selectivity. Prior to our studies, no compounds were reported that display significant selectivity between APH1A and APH1B complexes. The cellular assay at our disposal to pinpoint the complex selectivity allowed us to investigate the APH1 selectivity of known and newly synthesised compounds. Of newly synthesized compounds, ketones **12b** (9-fold), **12n** (13-fold), and **29d** (11-fold) displayed the highest selectivity towards PSEN1-APH1B compared to PSEN1-APH1A. The high selectivity was usually accompanied by a decrease in potency towards PSEN1-APH1B complex. For the more potent inhibitors, the selectivity ratio between PSEN1-APH1A and PSEN1-APH1B complex was between 2 to 6-fold (as observed in **13b-c** and **13k**).

Conclusion:

A ligand-based approach was used to understand the structural feature required for PSEN1 selectivity. Computational studies revealed that an aromatic sulfone /sulfonamide adopts unique “U” shape with an aryl group which is vital for PSEN1 selective inhibition. That led to the first rational design of [2,2,2]-azabicyclooctane sulphonamides as a new class of PSEN1 complex selective GSIs. The most potent compound (+)-**13b** displays 5.5 nM potency towards PSEN1-APH1B complex, little selectivity (~4-fold) towards PSEN1-APH1A complex and >300-fold selectivity versus PSEN2 complex. Also, (+) **13b** displayed good brain penetration following i.v. administration (with $K_{p,uu}$ around 2), good permeability with no indication of P-gp mediated efflux, moderate solubility, no cardiotoxicity (in preliminary assays), and weak CYP450 inhibition. Nevertheless, the high clearance of (+)-**13b** and high efflux ratio (32) of (+)-**21a** limited exploring compounds further in animal models. The excellent potency towards

PSEN1-APH1B complex and high selectivity versus PSEN2 complexes makes (+)-**13b** an excellent candidate for lead optimization. To the best of our knowledge, (+)-**13b** is one of the most potent γ -secretase inhibitors, rationally designed for selective inhibition of the PSEN1-APH1B complex to date. The availability of subcomplex specific assays combined with the obtained insight in the SAR for subcomplex selectivity sets the stage for developing a new generation of GSI tools and therapeutic agents.

EXPERIMENTAL SECTION

Chemistry:

All reactions were carried out by employing standard chemical techniques under inert atmosphere. Solvents used for extraction, washing, and chromatography were HPLC grade. Unless otherwise noted, all reagents were purchased from Sigma–Aldrich or Acros Organics and were used without further purification. All final compounds were characterized by ^1H , ^{13}C NMR and LC/MS. ^1H nuclear magnetic resonance spectra were recorded on Bruker spectrometers: 360 MHz and DPX–400 MHz. For the ^1H spectra, all chemical shifts are reported in part per million (δ) units and are relative to the residual signal at 7.26 and 2.50 ppm for CDCl_3 and DMSO, respectively. ^{13}C chemical shifts are reported as δ values in ppm relative to the residual solvent peak ($\text{CDCl}_3 = 77.16$). All final compounds were confirmed to be >95% pure via LCMS methods. All the LC/MS analyses were performed using an Agilent G1956A LC/MS quadrupole coupled to an Agilent 1100 series liquid chromatography (LC) system consisting of a binary pump with degasser, autosampler, thermostated column compartment, and diode array detector. The mass spectrometer (MS) was operated with an atmospheric pressure electrospray ionization (API–ES) source in positive ion mode. The capillary voltage was set to 3000 V and the fragmentor voltage to 70 V, and the quadrupole temperature was maintained at 100 °C. The drying gas flow and temperature values were 12.0 L/min and 350

°C, respectively. Nitrogen was used as the nebulizer gas at a pressure of 35 psi. Data acquisition was performed with Agilent Chemstation software. Analyses were carried out on a YMC pack ODS–AQ C18 column (50 mm long × 4.6 mm I.D.; 3 µm particle size) at 35 °C, with a flow rate of 2.6 mL/min. A gradient elution was performed from 95% (water + 0.1% formic acid)/5% acetonitrile to 5% (water + 0.1% formic acid)/95% acetonitrile in 4.8 min; the resulting composition was held for 1.0 min; from 5% (water + 0.1% formic acid)/95% acetonitrile to 95% (water + 0.1% formic acid)/5% acetonitrile in 0.2 min. The standard injection volume was 2 µL. Acquisition ranges were set to 190–400 nm for the UV–PDA detector and 100–1400 m/z for the MS detector. Optical rotations measurements were carried out on a 341 PerkinElmer polarimeter in the indicated solvents.

ELN-3184636³¹, **MRK-560**²⁹, and **ELN-475516**³² were synthesized based on the published procedures and were >95% pure as assessed by HPLC.

General procedure for aza–Diels–Alder reaction (A):

Benzaldehyde (1 equiv), *p*-anisidine (1 equiv) and 2-cyclohepten-1-one (1 equiv) in anhydrous DMF (15 mL) were placed in a microwave vial and 10 mol % of bismuth nitrate pentahydrate was added. The reaction vessel was placed in a microwave reactor and irradiated at 60 °C for 2 h. LCMS indicated the formation of *exo* and *endo* isomers. Reaction mixture was diluted with EtOAc (100 mL) and filtered through celite bed. The celite bed was washed with EtOAc several times and the filtrate was washed with water. The aqueous layer was extracted with EtOAc (3 × 50 mL). Combined organic layer was washed with water, brine, dried over anhydrous MgSO₄ and rotary evaporated. The residue was purified by flash column chromatography (0 to 7 % EtOAc in *n*-heptane) to afford the desired *exo* isomer.

***Exo-rac*–(1*S**,3*S**,4*S**)–2–(4-methoxyphenyl)–3–(4–(trifluoromethyl)phenyl)–2–azabicyclo[2.2.2]octan–5–one (9b)**

Synthesized using general procedure A. Starting from 4-trifluoromethyl benzaldehyde (1.57 mL, 11.486 mmol), 2-cyclohexen-1-one (1.112 mL, 11.486 mmol), *p*-anisidine (1.415 g, 11.486 mmol) and bismuth (III) nitrate pentahydrate (557 mg, 1.149 mmol) gave the titled compound (1.2 g, yield 27 %) as pale-yellow gummy solid.

¹H NMR (400 MHz, CDCl₃): δ = 7.64 (d, *J* = 8.14 Hz, 2H), 7.52–7.59 (m, 2H), 6.70–6.80 (m, 2H), 6.50–6.56 (m, 2H), 4.76 (d, *J* = 2.20 Hz, 1H), 4.44 (quin, *J* = 2.81 Hz, 1H), 3.71 (s, 3H), 2.78 (td, *J* = 3.08, 18.93 Hz, 1H), 2.67 (q, *J* = 2.86 Hz, 1H), 2.40 (dd, *J* = 1.76, 18.71 Hz, 1H), 2.18–2.30 (m, 1H), 1.85–1.97 (m, 1H), 1.66 (dt, *J* = 2.97, 8.20 Hz, 2H) ppm.

LC-MS *m/z*: 376 [M + H]⁺

General Procedure 4-methoxy phenyl (PMP) deprotection using CAN (B):

Substituted aryl-2-(4-methoxyphenyl)-2-azabicyclo[2.2.2]octan-5-one (1 eq) was dissolved in water and acetonitrile and the resulting mixture was cooled to 0 °C. To this ammonium cerium (IV) nitrate (2.5 eq) and H₂SO₄ (1M in water, 1 eq) were added and the reaction mixture was stirred for 1 h. After completion (TLC), reaction mixture was basified with 3 M KOH to the pH 9–10 and the suspension was filtered through dicalite bed. The dicalite bed was washed with EtOAc several times. Layers were separated and the aqueous layer was extracted with EtOAc (3 ×). Combined organic layer was washed with water, brine, dried over anhydrous MgSO₄, filtered and solvent was evaporated under reduced pressure. The crude residue was purified by flash column chromatography (10–25% EtOAc in *n*-heptane) to yield the desired amine.

***Rac-exo*-(1*S**,3*S**,4*S**)-3-(4-(trifluoromethyl)phenyl)-2-azabicyclo[2.2.2]octan-5-one (11b)**

Synthesized using general procedure B. Starting from *rac-exo*-(1*S**,3*S**,4*S**)-3-(4-(trifluoromethyl)phenyl)-2-azabicyclo[2.2.2]octan-5-one **9b** (2 g, 5.328 mmol),

ammonium cerium (IV) nitrate (7.302 g, 13.319 mmol) gave the titled compound (0.45 g, yield 31 %) as pale-brown gummy solid.

¹H NMR (400 MHz, CDCl₃): δ = 7.60–7.71 (m, 4H), 4.67 (s, 1H), 3.58 (tt, J = 1.93, 3.56 Hz, 1H), 2.58–2.67 (m, 1H), 2.43–2.52 (m, 2H), 2.05–2.19 (m, 1H), 1.65–1.80 (m, 2H), 1.51–1.61 (m, 2H) ppm.

LC-MS m/z : 270 [M + H]⁺

General Procedure for *N*-sulfonylation (D):

4-Chlorobenzene sulfonyl chloride (1.2 eq) was added in one portion to a stirred solution of aryl-2-azabicyclo[2.2.2]octan-5-one or aryl-2-azabicyclo[3.2.2]nonan-8-one (1 eq) and *N,N*-diisopropylethylamine (4 eq) in anhydrous dichloromethane at 0 °C. The resulting mixture reaction was warmed to ambient temperature continued stirring for 18 h. After completion (TLC and LCMS), reaction mixture was diluted with dichloromethane (40 mL) and washed with water. The aqueous layer was extracted with dichloromethane (2 ×). Combined organic layer was washed with water, brine, dried over anhydrous MgSO₄ and solvent was evaporated under reduced pressure. The residue obtained was purified by flash column chromatography (0–20% ethyl acetate in *n*-heptane) to afford the desired compound as colorless solid.

***Rac-exo*-(1*S**,3*S**,4*S**)-2-((4-chlorophenyl)sulfonyl)-3-(4-(trifluoromethyl)phenyl)-2-azabicyclo[2.2.2]octan-5-one (12b)**

Synthesized using general procedure D. Starting from 4-chlorobenzene sulfonyl chloride (517 mg, 2.451 mmol), *rac-exo*-(1*S**,3*S**,4*S**)-3-(4-(trifluoromethyl)phenyl)-2-azabicyclo[2.2.2]octan-5-one **11b** (550 mg, 2.043 mmol), DIPEA (1.408 mL, 8.17 mmol) gave the titled compound (650 mg, yield 71 %) as fluffy white solid.

^1H NMR (400 MHz, CDCl_3): δ = 7.64–7.69 (m, 2H), 7.61 (d, J = 8.36 Hz, 2H), 7.40–7.48 (m, 4H), 5.11–5.25 (m, 1H), 4.44–4.59 (m, 1H), 2.55 (q, J = 2.86 Hz, 1H), 2.37–2.47 (m, 1H), 2.21–2.34 (m, 2H), 1.79–1.93 (m, 1H), 1.67–1.78 (m, 1H), 1.56–1.66 (m, 1H) ppm.

LC-MS m/z : 441 $[\text{M} - \text{H}]^-$, 461 $[\text{M} + \text{NH}_4]^+$

General procedure for ketone reduction (E):

To a stirred solution of ketone (1 eq) in MeOH (6 mL), NaBH_4 (1 eq) was added in one portion and the resulting mixture was stirred at ambient temperature for 1 h. Upon completion (TLC), solvent was evaporated in vacuo, the residue was diluted with water and acidified with 1N HCl to pH = 4. The resulting mixture was extracted with EtOAc (3×25 mL). Combined organic phase was washed with water, brine, dried over anhydrous MgSO_4 and concentrated in vacuo. The residue was purified preparative HPLC (Stationary phase: RP XBridge Prep C18 ODB- $5\mu\text{m}$, 30×250 mm, Mobile phase: 0.25% NH_4HCO_3 solution in water, CH_3CN) to separate the diastereomers. to afford the desired 3-*endo* and 3-*exo* alcohols.

***Rac*-(1*S**,3*S**,4*S**,5*RS**)-2-((4-chlorophenyl)sulfonyl)-3-(4-(trifluoromethyl)phenyl)-2-azabicyclo[2.2.2]octan-5-ol**

Synthesized using general procedure E. Starting from *rac-exo*-(1*S**,3*S**,4*S**)-2-((4-chlorophenyl)sulfonyl)-3-(4-(trifluoromethyl)phenyl)-2-azabicyclo[2.2.2]octan-5-one **12b** (255 mg, 0.574 mmol), NaBH_4 (22 mg, 0.574 mmol) gave 3-*endo* and 3-*exo* alcohols.

***Rac-exo*-(1*S**,3*S**,4*S**,5*RS**)-2-((4-chlorophenyl)sulfonyl)-3-(4-(trifluoromethyl)phenyl)-2-azabicyclo[2.2.2]octan-5-ol (14b)**

100 mg (39 % yield), colorless solid.

^1H NMR (400 MHz, $\text{DMSO}-d_6$) δ = 7.86 (d, J = 8.58 Hz, 2H), 7.69 (s, 4H), 7.61–7.66 (m, 2H), 4.83–4.90 (m, 2H), 3.89 (br d, J = 1.76 Hz, 1H), 3.58–3.65 (m, 1H), 1.79–1.90 (m, 2H), 1.56–1.72 (m, 3H), 1.08 (dd, J = 4.18, 13.86 Hz, 1H), 0.92 (br t, J = 10.78 Hz, 1H) ppm.

^{13}C NMR (101 MHz, DMSO- D_6) δ = 146.8 (s), 138.1 (s), 137.9 (s), 129.5 (s), 129.3 (s), 127.4 (s), 127.0 (s), 126.9 (s), 124.6 – 124.9 (m), 66.1 (s), 60.5 (s), 47.7 (s), 40.7 (s), 34.7 (s), 27.0 (s), 10.8 (s) ppm.

LC-MS m/z : 444 $[\text{M} - \text{H}]^-$, 463 $[\text{M} + \text{NH}_4]^+$

Rac-endo-(1S*,3S*,4S*5RS*)-2-((4-chlorophenyl)sulfonyl)-3-(4-(trifluoromethyl)phenyl)-2-azabicyclo[2.2.2]octan-5-ol (13b)

125 mg (48 % yield), colorless solid.

^1H NMR (400 MHz, DMSO- D_6) δ = 7.78 (d, J = 8.80 Hz, 2H), 7.70 (d, J = 8.14 Hz, 2H), 7.65 (d, J = 8.80 Hz, 2H), 7.54 (d, J = 8.14 Hz, 2H), 5.15 (s, 1H), 4.81 (d, J = 2.20 Hz, 1H), 3.94 (br s, 1H), 3.75–3.86 (m, 1H), 1.84–1.98 (m, 1H), 1.76–1.84 (m, 1H), 1.70 (ddd, J = 1.54, 9.68, 14.08 Hz, 1H), 1.44–1.57 (m, 1H), 1.21–1.32 (m, 1H), 1.12–1.21 (m, 1H), 1.04–1.12 (m, 1H) ppm.

^{13}C NMR (101 MHz, DMSO- D_6) δ = 147.5 (s), 138.2 (s), 137.8 (s), 129.4 (s), 129.3 (s), 127.2 (s), 126.9 (s), 125.7 (s), 124.8 (q, J = 3.3 Hz), 64.6 (s), 55.2 (s), 47.4 (s), 41.2 (s), 34.5 (s), 25.9 (s), 15.4 (s) ppm.

LC-MS m/z : 444 $[\text{M} - \text{H}]^-$, 463 $[\text{M} + \text{NH}_4]^+$

Biology:

Generation of Stable Cell Lines:

Conditional *Psen1/2* double knock-out mice were crossed with conditional *Aph1ABC* triple knock-out mice. At embryonic day 7.5, embryos were dissected and dissociated, and cells were plated in the presence of DMEM/F12 50% FCS (Invitrogen). Primary mouse embryonic fibroblasts (MEFs) were immortalized by transduction with LargeT antigen. *Psen1/2* double knockout/*Aph1ABC* triple knock-out MEFs were generated by transduction with a Cre-GFP expressing adenoviral vector and GFP-positive MEFs were sorted by FACS analysis. *Psen1/2* *Aph1ABC*-deficient MEFs were maintained in DMEM/f12 10% FCS. To rescue γ -secretase

expression, Psen1/2 double knock-out/Aph1ABC triple knock-out MEFs were transduced using pMSCV viral vectors (Clontech) containing the human coding sequences of the different PSEN and APH1 homologues and the zeocin selection marker. An IRES sequence was cloned between the coding sequences for PSEN and APH1 to ensure co-expression of both proteins. Stable transfected cell lines were selected using 500 µg/ml zeocin (Invitrogen). Four different combinations were made: PSEN1 and APH1A_L, PSEN1 and APH1B, PSEN2 and APH1A_L, and PSEN2 and APH1B. These cell lines were transduced with pMSCV viral vectors (Clontech) expressing APP-C99-GFP-puromycin. After puromycin selection (5 µg/ml), GFP-positive cells were selected through FACS sorting. For the alanine mutagenesis experiment pMSCV PSEN1-APH1A viral vectors were generated by long PCR-based QuikChange strategy (Stratagene). Stable cell lines were generated for each mutant as described above.

Testing compounds

The number of plated cells and incubation times were determined in respect of linearity of A β peptide secretion, the dynamic range of A β peptide quantification in the medium, and sensitivity to DMSO. In every plate avagacestat was tested at 10 µM to determine the noise signal by completely blocking γ -secretase (See also Appendix Fig S2). MEF cells were plated in DMEM F12 supplemented with 10% FCS at 10,000 cells per well in 96 clear bottom well plates in the late afternoon and cultured for 16 h at 37°C, 5 % CO₂. In the morning of the second day, medium was replaced with 60 µl DMEM/F12 supplemented with 2% FCS and GSI or DMSO (controls) were added. Compounds were tested in serial dilutions with concentrations ranging from 10 mM to 0.1 nM with 3-fold changes. Final concentration of DMSO in all wells was 0.2%. Plates were put in the incubator again at 37°C, 5% CO₂. After 8h, the culture media were collected and 30 µl was used to measure A β 40 peptides. The cell viability was assessed using the CellTiter-Glo Luminescent assay (Promega) that measures ATP production. All screens were performed at one site and reported IC₅₀ values throughout

the manuscript are from this site (Beerse) unless otherwise indicated. We however measured 5 compounds at the Leuven site and noticed that absolute IC₅₀ values were different (Appendix Fig. S2). The main goal of the current work is to explore the basis for inhibitor selectivity for different γ -secretases and selectivity was consistent in the assays at the two sites (Appendix Fig S2).

Quantification of soluble A β peptides using ELISA

Standard 96 well SECTOR plates (MSD) were coated with 1.5 μ g/ml anti-A β JRFcA β 40/28 capture antibody in a final volume of 50 μ L of PBS 0.05% Tween 20. After overnight incubation at 4 °C, the plates were 5 times rinsed with PBS 0.05% Tween 20 and blocked with 150 μ L per well of casein buffer (PBS with 1% casein, pH 7.4) for 4 h at room temperature. Standards (synthetic human A β 1–40) were diluted in culture media. Standards and samples were preincubated with JRFA β N/25 (human specific antibody) labeled with sulfo-TAG detection antibody in casein buffer for 5' at room temperature. The blocked assay plate was rinsed 5 times with PBS 0.05% Tween 20 and the sample and secondary antibody mix was added. After overnight incubation at 4 °C, plates were rinsed with PBS 0.05% Tween 20 and 150 μ L 2 \times Rad T buffer (MSD) was added and plates were read on a MSD Sector S 600 reader without any delay.

Data calculation

For each MEF cell line, A β peptide levels are expressed as % of the signal measured for DMSO (control) after subtraction of the signal obtained in the presence of 10 μ M avagacestat, that is supposed to completely block all γ -secretase activity. Typical signal to noise ratios were >10. Z prime scores in all experiments were well above 0.6. GraphPad Prism 7 software was used to generate inhibition fitting curves (four-parameter logistic equation, non-linear regression) and to determine IC₅₀ values and 95%CI.

CYP450 Inhibition Assay.

The potential to reversibly inhibit the major human P450 isoforms (CYPs 1A2, 2C9, 2C19, 2D6, and 3A4) was determined using recombinantly expressed human CYPs. Specific probe substrates were used for each CYP isoform which were known to be selectively metabolized to defined fluorescent metabolites. Each test compound was incubated with individual CYPs over a concentration range up to 10 μ M. At the end of the incubation, the level of fluorescence was measured on a plate reader. The level of fluorescence in the presence and absence of test compound was used to determine the IC₅₀ against each CYP isoform.

Plasma protein binding assay.

The free fraction in mouse and human plasma was determined by Rapid Equilibrium Dialysis (RED Device, Thermo Fisher Scientific, Geel, Belgium). The RED device consists of a 48 well plate containing disposable inserts bisected by a semi-permeable membrane creating two chambers. A 300 μ L aliquot of plasma containing test compound at 5 μ M was placed one side and 500 μ L of phosphate buffered saline (PBS) the other. The plate was sealed and incubated at approximately 37 °C for 4.5 h. After 4.5 h samples were removed and both the plasma and buffer compartment and analyzed for test compound using a specific HPLC-MS/MS method to estimate free and bound concentrations.

Non-specific binding to brain tissue assay.

The *in vitro* non-specific binding of compounds to rat brain homogenate was determined using the RED Device (see above). Each test compound was diluted with rat brain homogenate, prepared following a 1:10 dilution with PBS, to achieve a final concentration of 5 μ M. The plate was incubated at approximately 37 °C for 5 h. After 5 h samples were removed from both the brain homogenate and buffer compartment and analyzed for test compound using a specific HPLC-MS/MS method to estimate free and bound concentrations.

***In vitro* permeability/P-gp efflux assay.**

The in vitro permeability and potential to be transported by P-glycoprotein (P-gp) was determined using an LLC cell line transfected with human MDR1 (P-glycoprotein). Each test compound (5 μ M) was added to either the apical (A) side of a confluent monolayer of LLC-MDR1 cells and permeability towards the basolateral (B) direction measured by monitoring the appearance of the test compound on the opposite side of the membrane using a specific LC-MS/MS method. Permeability was assessed in with and without elacridar (GF 120918, CAS 143851-98-3), a well-known P-gp inhibitor. The A>B+elacridar/A>B-elacridar ratio (P_{app} ratio) was calculated and used to determine if the test compound was subject to efflux by P-gp.

Acknowledgements

This work has been funded by a 2017 VLAIO grant (Project SELGAM – ICD1052701, ICD1134808). The work was supported by an AIO-project (no. HBC.2016.0884). This work was supported by the Flanders Institute for Biotechnology (VIB vzw), a Methusalem grant from KU Leuven and the Flemish Government, the Fonds voor Wetenschappelijk Onderzoek, KU Leuven, The Queen Elisabeth Medical Foundation for Neurosciences, the Opening the Future campaign of the Leuven Universitair Fonds, the Belgian Alzheimer Research Foundation (SAO-FRA) and the Alzheimer's Association USA. B.D.S. holds the Bax-Vanluffelen Chair for Alzheimer's Disease.

Supporting Information Available: Experimental details of all the tested compounds and their intermediates described in this paper, synthetic procedures, ^1H NMR, ^{13}C NMR and spectroscopic data.

References:

1. Li, Y. M.; Lai, M. T.; Xu, M.; Huang, Q.; DiMuzio-Mower, J.; Sardana, M. K.; Shi, X. P.; Yin, K. C.; Shafer, J. A.; Gardell, S. J. Presenilin 1 is linked with gamma-secretase

- activity in the detergent solubilized state. *Proc. Natl. Acad. Sci. USA* **2000**, 97, 6138-43.
2. Yu, G.; Nishimura, M.; Arawaka, S.; Levitan, D.; Zhang, L.; Tandon, A.; Song, Y. Q.; Rogaeva, E.; Chen, F.; Kawarai, T.; Supala, A.; Levesque, L.; Yu, H.; Yang, D. S.; Holmes, E.; Milman, P.; Liang, Y.; Zhang, D. M.; Xu, D. H.; Sato, C.; Rogae, E.; Smith, M.; Janus, C.; Zhang, Y.; Aebersold, R.; Farrer, L. S.; Sorbi, S.; Bruni, A.; Fraser, P.; St George-Hyslop, P. Nicastrin modulates presenilin-mediated notch/glp-1 signal transduction and betaAPP processing. *Nature* **2000**, 407, 48-54.
 3. Francis, R.; McGrath, G.; Zhang, J.; Ruddy, D. A.; Sym, M.; Apfeld, J.; Nicoll, M.; Maxwell, M.; Hai, B.; Ellis, M. C.; Parks, A. L.; Xu, W.; Li, J.; Gurney, M.; Myers, R. L.; Himes, C. S.; Hiebsch, R.; Ruble, C.; Nye, J. S.; Curtis, D. aph-1 and pen-2 are required for Notch pathway signaling, gamma-secretase cleavage of betaAPP, and presenilin protein accumulation. *Dev. Cell* **2002**, 3, 85-97.
 4. Goutte, C.; Tsunozaki, M.; Hale, V. A.; Priess, J. R. APH-1 is a multipass membrane protein essential for the Notch signaling pathway in *Caenorhabditis elegans* embryos. *Proc. Natl. Acad. Sci. USA* **2002**, 99, 775-9.
 5. De Strooper, B. Aph-1, Pen-2, and Nicastrin with Presenilin generate an active gamma-Secretase complex. *Neuron* **2003**, 38, 9-12.
 6. Wolfe, M. S.; Xia, W.; Ostaszewski, B. L.; Diehl, T. S.; Kimberly, W. T.; Selkoe, D. J. Two transmembrane aspartates in presenilin-1 required for presenilin endoproteolysis and gamma-secretase activity. *Nature* **1999**, 398, 513-7.
 7. Ahn, K.; Shelton, C. C.; Tian, Y.; Zhang, X.; Gilchrist, M. L.; Sisodia, S. S.; Li, Y. M. Activation and intrinsic gamma-secretase activity of presenilin 1. *Proc. Natl. Acad. Sci. USA* **2010**, 107, 21435-40.

8. De Strooper, B. Lessons from a failed gamma-secretase Alzheimer trial. *Cell* **2014**, 159, 721-6.
9. Serneels, L.; Van Biervliet, J.; Craessaerts, K.; Dejaegere, T.; Horre, K.; Van Houtvin, T.; Esselmann, H.; Paul, S.; Schafer, M. K.; Berezovska, O.; Hyman, B. T.; Sprangers, B.; Sciot, R.; Moons, L.; Jucker, M.; Yang, Z.; May, P. C.; Karran, E.; Wiltfang, J.; D'Hooge, R.; De Strooper, B. gamma-Secretase heterogeneity in the Aph1 subunit: relevance for Alzheimer's disease. *Science* **2009**, 324, 639-42.
10. Karran, E.; Mercken, M.; De Strooper, B. The amyloid cascade hypothesis for Alzheimer's disease: an appraisal for the development of therapeutics. *Nat. Rev. Drug. Discov.* **2011**, 10, 698-712.
11. Selkoe, D. J. Alzheimer's disease: genes, proteins, and therapy. *Physiol. Rev.* **2001**, 81, 741-66.
12. Selkoe, D. J.; Hardy, J. The amyloid hypothesis of Alzheimer's disease at 25 years. *EMBO Mol. Med.* **2016**, 8, 595-608.
13. De Strooper, B.; Karran, E. The Cellular Phase of Alzheimer's Disease. *Cell* **2016**, 164, 603-15.
14. De Strooper, B.; Saftig, P.; Craessaerts, K.; Vanderstichele, H.; Guhde, G.; Annaert, W.; Von Figura, K.; Van Leuven, F. Deficiency of presenilin-1 inhibits the normal cleavage of amyloid precursor protein. *Nature* **1998**, 391, 387-90.
15. De Strooper, B.; Annaert, W.; Cupers, P.; Saftig, P.; Craessaerts, K.; Mumm, J. S.; Schroeter, E. H.; Schrijvers, V.; Wolfe, M. S.; Ray, W. J.; Goate, A.; Kopan, R. A presenilin-1-dependent gamma-secretase-like protease mediates release of Notch intracellular domain. *Nature* **1999**, 398, 518-22.
16. Struhl, G.; Greenwald, I. Presenilin is required for activity and nuclear access of Notch in *Drosophila*. *Nature* **1999**, 398, 522-5.

17. Saito, T.; Suemoto, T.; Brouwers, N.; Sleegers, K.; Funamoto, S.; Mihira, N.; Matsuba, Y.; Yamada, K.; Nilsson, P.; Takano, J.; Nishimura, M.; Iwata, N.; Van Broeckhoven, C.; Ihara, Y.; Saido, T. C. Potent amyloidogenicity and pathogenicity of Abeta43. *Nat. Neurosci.* **2011**, 14, 1023-32.
18. Veugelen, S.; Saito, T.; Saido, T. C.; Chavez-Gutierrez, L.; De Strooper, B. Familial Alzheimer's Disease Mutations in Presenilin Generate Amyloidogenic Abeta Peptide Seeds. *Neuron* **2016**, 90, 410-6.
19. Szaruga, M.; Munteanu, B.; Lismont, S.; Veugelen, S.; Horre, K.; Mercken, M.; Saido, T. C.; Ryan, N. S.; De Vos, T.; Savvides, S. N.; Gallardo, R.; Schymkowitz, J.; Rousseau, F.; Fox, N. C.; Hopf, C.; De Strooper, B.; Chavez-Gutierrez, L. Alzheimer's-Causing Mutations Shift Abeta Length by Destabilizing gamma-Secretase-Abeta Interactions. *Cell* **2017**, 170, 443-456 e14.
20. Vandersteen, A.; Masman, M. F.; De Baets, G.; Jonckheere, W.; van der Werf, K.; Marrink, S. J.; Rozenski, J.; Benilova, I.; De Strooper, B.; Subramaniam, V.; Schymkowitz, J.; Rousseau, F.; Broersen, K. Molecular plasticity regulates oligomerization and cytotoxicity of the multi-peptide-length amyloid-beta peptide pool. *J. Biol. Chem.* **2012**, 287, 36732-43.
21. Haapasalo, A.; Kovacs, D. M. The many substrates of presenilin/gamma-secretase. *J. Alzheimers Dis.* **2011**, 25, 3-28.
22. Doody, R. S.; Raman, R.; Farlow, M.; Iwatsubo, T.; Vellas, B.; Joffe, S.; Kieburtz, K.; He, F.; Sun, X.; Thomas, R. G.; Aisen, P. S.; Alzheimer's Disease Cooperative Study Steering, C.; Siemers, E.; Sethuraman, G.; Mohs, R.; Semagacestat Study, G. A phase 3 trial of semagacestat for treatment of Alzheimer's disease. *N. Engl. J. Med.* **2013**, 369, 341-50.

23. Krop, I.; Demuth, T.; Guthrie, T.; Wen, P. Y.; Mason, W. P.; Chinnaiyan, P.; Butowski, N.; Groves, M. D.; Kesari, S.; Freedman, S. J.; Blackman, S.; Watters, J.; Loboda, A.; Podtelezhnikov, A.; Lunceford, J.; Chen, C.; Giannotti, M.; Hing, J.; Beckman, R.; Lorusso, P. Phase I pharmacologic and pharmacodynamic study of the gamma secretase (Notch) inhibitor MK-0752 in adult patients with advanced solid tumors. *J. Clin. Oncol.* **2012**, 30, 2307-13.
24. Habets, R. A.; de Bock, C. E.; Serneels, L.; Lodewijckx, I.; Verbeke, D.; Nittner, D.; Narlawar, R.; Demeyer, S.; Dooley, J.; Liston, A.; Taghon, T.; Cools, J.; de Strooper, B. Safe targeting of T cell acute lymphoblastic leukemia by pathology-specific NOTCH inhibition. *Sci. Transl. Med.* **2019**, 11, eaau6246.
25. Schott, A. F.; Landis, M. D.; Dontu, G.; Griffith, K. A.; Layman, R. M.; Krop, I.; Paskett, L. A.; Wong, H.; Dobrolecki, L. E.; Lewis, M. T.; Froehlich, A. M.; Paraniham, J.; Hayes, D. F.; Wicha, M. S.; Chang, J. C. Preclinical and clinical studies of gamma secretase inhibitors with docetaxel on human breast tumors. *Clin. Cancer. Res.* **2013**, 19, 1512-24.
26. Churcher, I.; Beher, D.; Best, J. D.; Castro, J. L.; Clarke, E. E.; Gentry, A.; Harrison, T.; Hitzel, L.; Kay, E.; Kerrad, S.; Lewis, H. D.; Morentin-Gutierrez, P.; Mortishire-Smith, R.; Oakley, P. J.; Reilly, M.; Shaw, D. E.; Shearman, M. S.; Teall, M. R.; Williams, S.; Wrigley, J. D. 4-substituted cyclohexyl sulfones as potent, orally active gamma-secretase inhibitors. *Bioorg. Med. Chem. Lett.* **2006**, 16, 280-4.
27. Best, J. D.; Jay, M. T.; Otu, F.; Churcher, I.; Reilly, M.; Morentin-Gutierrez, P.; Pattison, C.; Harrison, T.; Shearman, M. S.; Atack, J. R. In vivo characterization of Abeta(40) changes in brain and cerebrospinal fluid using the novel gamma-secretase inhibitor N-[cis-4-[(4-chlorophenyl)sulfonyl]-4-(2,5-difluorophenyl)cyclohexyl]-

- 1,1,1-trifluoromethanesulfonamide (MRK-560) in the rat. *J. Pharmacol. Exp. Ther.* **2006**, 317, 786-90.
28. Best, J. D.; Smith, D. W.; Reilly, M. A.; O'Donnell, R.; Lewis, H. D.; Ellis, S.; Wilkie, N.; Rosahl, T. W.; Laroque, P. A.; Boussiquet-Leroux, C.; Churcher, I.; Atack, J. R.; Harrison, T.; Shearman, M. S. The novel gamma secretase inhibitor N-[cis-4-[(4-chlorophenyl)sulfonyl]-4-(2,5-difluorophenyl)cyclohexyl]-1,1,1-trifluoromethanesulfonamide (MRK-560) reduces amyloid plaque deposition without evidence of notch-related pathology in the Tg2576 mouse. *J. Pharmacol. Exp. Ther.* **2007**, 320, 552-8.
29. Lee, J.; Song, L.; Terracina, G.; Bara, T.; Josien, H.; Asberom, T.; Sasikumar, T. K.; Burnett, D. A.; Clader, J.; Parker, E. M.; Zhang, L. Identification of presenilin 1-selective gamma-secretase inhibitors with reconstituted gamma-secretase complexes. *Biochemistry* **2011**, 50, 4973-80.
30. Borgegard, T.; Gustavsson, S.; Nilsson, C.; Pärpal, S.; Klintonberg, R.; Berg, A. L.; Rosqvist, S.; Serneels, L.; Svensson, S.; Olsson, F.; Jin, S.; Yan, H.; Wanngren, J.; Jureus, A.; Ridderstad-Wollberg, A.; Wollberg, P.; Stockling, K.; Karlstrom, H.; Malmberg, A.; Lund, J.; Arvidsson, P. I.; De Strooper, B.; Lendahl, U.; Lundkvist, J. Alzheimer's disease: presenilin 2-sparing gamma-secretase inhibition is a tolerable Abeta peptide-lowering strategy. *J. Neurosci.* **2012**, 32, 17297-305.
31. Wu, W. L.; Domalski, M.; Burnett, D. A.; Josien, H.; Bara, T.; Rajagopalan, M.; Xu, R.; Clader, J.; Greenlee, W. J.; Brunskill, A.; Hyde, L. A.; Del Vecchio, R. A.; Cohen-Williams, M. E.; Song, L.; Lee, J.; Terracina, G.; Zhang, Q.; Nomeir, A.; Parker, E. M.; Zhang, L. Discovery of SCH 900229, a Potent Presenilin 1 Selective gamma-Secretase Inhibitor for the Treatment of Alzheimer's Disease. *ACS Med. Chem. Lett.* **2012**, 3, 892-6.

32. Zhao, B.; Yu, M.; Neitzel, M.; Marugg, J.; Jagodzinski, J.; Lee, M.; Hu, K.; Schenk, D.; Yednock, T.; Basi, G. Identification of gamma-secretase inhibitor potency determinants on presenilin. *J. Biol. Chem.* **2008**, 283, 2927-38.
33. Teall, M.; Oakley, P.; Harrison, T.; Shaw, D.; Kay, E.; Elliott, J.; Gerhard, U.; Castro, J. L.; Shearman, M.; Ball, R. G.; Tsou, N. N. Aryl sulfones: a new class of gamma-secretase inhibitors. *Bioorg. Med. Chem. Lett.* **2005**, 15, 2685-8.
34. Xu, R.; Cole, D.; Asberom, T.; Bara, T.; Bennett, C.; Burnett, D. A.; Clader, J.; Domalski, M.; Greenlee, W.; Hyde, L.; Josien, H.; Li, H.; McBriar, M.; McKittrick, B.; McPhail, A. T.; Pissarnitski, D.; Qiang, L.; Rajagopalan, M.; Sasikumar, T.; Su, J.; Tang, H.; Wu, W. L.; Zhang, L.; Zhao, Z. Design and synthesis of tricyclic sulfones as gamma-secretase inhibitors with greatly reduced Notch toxicity. *Bioorg. Med. Chem. Lett.* **2010**, 20, 2591-6.
35. Mattson, M. N.; Neitzel, M. L.; Quincy, D. A.; Semko, C. M.; Garofalo, A. W.; Keim, P. S.; Konradi, A. W.; Pleiss, M. A.; Sham, H. L.; Brigham, E. F.; Goldbach, E. G.; Zhang, H.; Sauer, J. M.; Basi, G. S. Discovery of sulfonamide-pyrazole gamma-secretase inhibitors. *Bioorg. Med. Chem. Lett.* **2010**, 20, 2148-50.
36. Serneels, L.; Narlawar, R.; Perez-Benito, L; Municoy, M.; Guallar, V.; T'Syen, D.; Dewilde, M.; Bischoff, F.; Fraiponts, E.; Tresadern, G.; Roevens, P.W.M.; Gijzen, H. J. M.; De Strooper, B. Selective inhibitors of the PSEN1-gamma-secretase complex. *J Biol Chem* **2023**, 299, 104794.
37. Ram Naresh, Y.; Ashwini, B.; Sunena, C.; Bimal, K. B. Bismuth Nitrate Catalyzed Microwave Assisted Aza-Diels Alder Reaction for Synthesis of Bicyclo[2,2,2]-Octanones Scaffold. *Curr. Microwave Chem.* **2014**, 1, 94-97.

38. Verkade, J. M. M.; van Hemert, L. J. C.; Quaedflieg, P. J. L. M.; Alsters, P. L.; van Delft, F. L.; Rutjes, F. P. J. T. Mild and efficient deprotection of the amine protecting p-methoxyphenyl (PMP) group. *Tet. Lett.* **2006**, 47, 8109-8113.
39. Zhao, Z.; Pissarnitski, D. A.; Josien, H. B.; Wu, W. L.; Xu, R.; Li, H.; Clader, J. W.; Burnett, D. A.; Terracina, G.; Hyde, L.; Lee, J.; Song, L.; Zhang, L.; Parker, E. M. Discovery of a Novel, Potent Spirocyclic Series of gamma-Secretase Inhibitors. *J Med Chem* **2015**, 58, 8806-17.

Highlights:

- Selective inhibition of PSEN1 selective γ -secretase complexes have been shown to be efficacious while overcoming side effects observed with non-selective γ -secretase inhibition.
- Conformational modeling studies with known PSEN1 selective inhibitors revealed that a characteristic 'U' shape orientation between aromatic sulfone/sulfonamide and aryl ring is crucial for PSEN-1 selectivity and potency.
- 2-azabicyclo[2.2.2]octane sulfonamides provided potent PSEN1 selective inhibitors with low nanomolar potency towards PSEN1-APH1B complex.
- **(+)-13b** displayed low nanomolar potency towards the PSEN1-APH1B complex, high PSEN2 selectivity, excellent brain penetration, no significant CYP inhibition, or cardiotoxicity, good solubility, and permeability.

Declaration of interest statement:

Rajeshwar Narlawar, Lutgarde Serneels, Celia Gaffric, François Bischoff, Harrie J. M. Gijzen declare no competing interest. Bart De Strooper is or has been a consultant for Eli Lilly, Biogen, Janssen Pharmaceutica, Eisai, AbbVie and other companies. B.D.S is also a scientific founder of Augustine Therapeutics and a scientific founder and stockholder of Muna Therapeutics.